J Solid State Electrochem (1999) 3: 61–81

REVIEW

Vladislav V. Kharton · Evgeny N. Naumovich
Alim A. Vecher

Research on the electrochemistry of oxygen ion conductors in the former Soviet Union. I. ZrO_2-based ceramic materials

Received: 26 March 1998 / Accepted: 4 June 1998

Abstract Developments of solid electrolytes and mixed conductors based on stabilized zirconia in the former Soviet Union are reviewed. Primary attention is given to experimental data on high-conducting electrolytes, mixed conductors obtained by doping zirconia with transition metal oxides, oxygen exchange and oxygen permeation processes, as well as properties of metal electrodes in contact with the stabilized zirconia.

Key words Stabilized zirconia · Ionic conductivity · Mixed conductors · Oxygen permeation · Electrode

Introduction

Oxide materials with oxygen ionic and mixed ionic-electronic conductivity have a wide application in high-temperature electrochemical devices such as solid oxide fuel cells (SOFCs), oxygen separation membranes, membrane reactors for hydrocarbon oxidation, and sensors. Therefore the development of oxides having satisfactory properties for electrochemical devices is very important. However, numerous studies of materials and electrochemical cells with oxygen ionic conductors performed in the former Soviet Union are still unknown to Western scientists. The present work is aimed at reviewing these developments in order to facilitate access to the wealth of publication which have appeared in Russian. Most attention is given to the results which could be of interest at the present time from the viewpoint of developing electrochemical devices. In addition to the most interesting research projects, we made an attempt to briefly list articles published in less-known journals to assist in searching for information useful for researchers. The authors did not try to compare the results obtained in the Soviet Union and in Western scientific centers or to draw any analogies.

This is the first part of a series of reviews. It is focused on experimental data on solid electrolytes and mixed conductors based on stabilized zirconia and the electrochemical properties of such materials. Following parts will be devoted to perovskites (part II), oxide compounds based on bismuth oxide, ceria, thoria, and hafnia (part III), pyrochlores and ion-conducting oxide phases of other structural types (part IV), and finally on applications of oxygen ionic conductors (part V).

V.V. Kharton (✉) · E.N. Naumovich · A.A. Vecher
Institute of Physicochemical Problems
Belarus State University,
14 Leningradskaya Str., 220080 Minsk,
Republic of Belarus
e-mail: kharton@fhp.bsu.unibel.by or nen@basnet.minsk.by
Tel.: +375-17-220 76 81, Fax: +375-17-226 46 96

Solid electrolytes based on ZrO_2

The main requirements for solid oxide electrolyte materials determining their applicability are high ionic conductivity with negligible electronic conduction and thermodynamic stability under the conditions of the application, and an absence of the degradation of the transport property with time. In known oxide systems based on zirconium dioxide, solid solutions with the cubic fluorite-type structure satisfy these requirements to a large extent [1–3]. Existence of such solid solutions at temperatures below 1000 °C is characteristic of the binary oxide systems ZrO_2-Me_2O_3 (where Me is a rare-earth element) and ZrO_2-CaO [4, 5].

The binary oxide systems ZrO_2-Me_2O_3 (Me = La, Nd-Lu, Y, Sc)

Phase relationships

Phase diagrams, selected relationships between chemical and phase compositions, or the structure of separate phases were studied for the systems ZrO_2-Sc_2O_3 [6–11],

ZrO_2-Y_2O_3 [12–17], ZrO_2-La_2O_3 [18–20], ZrO_2-Ce_2O_3 (CeO_2) [21–24], ZrO_2-PrO_x [25–29], ZrO_2-Nd_2O_3 [18, 30–38], ZrO_2-Sm_2O_3 [33, 34], ZrO_2-Eu_2O_3 [34, 39], ZrO_2-Gd_2O_3 [34, 40], ZrO_2-Dy_2O_3 [33, 34, 37, 38, 40], ZrO_2-Ho_2O_3 [40], ZrO_2-Er_2O_3 [40], ZrO_2-Tm_2O_3 [40], ZrO_2-Yb_2O_3 [7, 33, 34, 40], and ZrO_2-Lu_2O_3 [40]. Ranges of formation of the cubic fluorite solid solutions (F-phase) were found for all these systems. There are also fields of tetragonal (T) and monoclinic (M) phases and co-existing phase mixtures in zirconia-rich parts of the phase diagrams. For the ZrO_2-Me_2O_3 systems with a large radius of the rare-earth cation (Me = La-Gd), a typical feature is the formation of the pyrochlore phase $Me_2Zr_2O_7$ and solid solutions based on it [18–20, 27–32, 35, 36, 41–43]. A decreasing radius of the dopant cation is observed to decrease the pyrochlore phase stability and to enlarge the temperature and concentration limits of the existing F-phase. For example, the fluorite-type solid solutions in the ZrO_2-La_2O_3 system exist in a narrow composition range and are unstable at temperatures below 1900 °C. If the $LaO_{1.5}$ content is less than 50 mol% the ceramics of ZrO_2-La_2O_3 represents a mixture of the T-phase with the cubic pyrochlore $La_2Zr_2O_7$. At the same time, the range of formation of the formation of the fluorite solid solution the system ZrO_2-Y_2O_3 is up to 50–60 mol% $YO_{1.5}$ at 1250 °C and increases significantly with increasing temperature.

One should note that numerous literature data on phase composition of the oxides at temperatures below 1200–1400 °C diverge considerably. This is caused by a low rate of the solid-state synthesis and phase decomposition process [41]. As a result, the phase composition of the ceramics at medium temperatures represents a function of the preparation conditions. For instance, the fluorite-type cubic solid solutions ZrO_2-Y_2O_3 may be obtained by a synthesis from organometallic compounds at a yttria content up to 4.5 mol% at temperatures of 600-800 °C [44, 45]. Analogously, preparing complex oxides of the system ZrO_2-Nd_2O_3 by coprecipitation or by thermal decomposition of nitrates leads to the formation of metastable cubic solid solutions, the structure of which changes continuously from fluorite through pyrochlore to Mn_2O_3 type (C-form of neodymia) [31, 32]. Increasing the temperature results, however, in a decomposition of the metastable F-phase forming thermodynamically stable phases (Scheme 1) [32]:

Electrical conductivity of the fluorites

A large number of research projects showed that the conductivity of the fluorite-type solutions has a maximum at 8–10 mol% $MeO_{1.5}$ (Me = Nd-Lu, Y, Sc) and decreases with further increases in dopant concentration [7, 8, 14, 35, 37, 38, 40, 46–52]. Therefore a position of the maximum in the conductivity versus composition curves is close to a minimum dopant concentration which provides stabilization of the F-phase at temperatures below 1000 °C (low limit of the stabilization) [40]. Notice that (1) the dopant content corresponding to the conductivity maximum may be somewhat higher compared to the low stabilization limit, and (2) both these concentration values depend on the conditions of processing the ceramics. Table 1 presents selected data on electrical properties of the zirconia-based solid electrolytes having the highest conductivity prepared by different methods.

The results of systematic studies of the conductivity of zirconia stabilized by Gd, Dy, Ho, Er, Tm, Yb, Lu, Y, and Sc have been presented and analyzed [40]. All the ceramic electrolytes were obtained using a uniform method (co-precipitation of the hydroxides with subsequent sintering). The minimum dopant concentration to stabilize the fluorite phase in the systems ZrO_2-$MeO_{1.5}$ (ME = Gd, Dy, Ho, Er, Tm, Yb, Lu) was found to be about 7.0–8.5 mol% of the stabilizing addition, being essentially independent of temperature. The conductivity maximum in all the systems closely coincides with the existing F-phase limit. The conductivity increases linearly with decreasing ionic radius of the dopant in the sequence $Nd < Gd < Dy < Ho \approx Y < Er < Yb < Lu < Sc$ (Fig. 1). Analogously to the low stabilization limit, the conductivity maximum in each of the systems is observed to be independent of temperature.

Temperature dependences of the conductivity of the $Zr_{0.90}Me_{0.10}O_{1.95}$ electrolytes can be approximated by several linear segments in the Arrhenius diagrams, whereas a curvature of these dependencies increases with increasing conductivity [53]. The activation energy for electrical conduction at temperatures above 1200 °C was found to decrease with decreasing radii of the dopant cations. At lower temperatures, the dependencies of conductivity on composition are more complex. It was shown experimentally that the breaks in the conductivity versus reciprocal temperature curves for the ceramics

$$Zr_{0.82}Nd_{0.18}O_{1.91}(cub) \xrightarrow{1100\text{–}1200\ ^\circ C} \underset{\text{(cubic fluorite)}}{Zr_{0.75}Nd_{0.25}O_{1.87}} + \underset{\text{(cubic fluorite)}}{Zr_{0.96}Nd_{0.04}O_{1.98}}$$

$$\downarrow\ 1200\text{–}1300\ ^\circ C \qquad \downarrow$$

$$\underset{\text{(pyrochlore)}}{Nd_{0.98}Zr_{3.02}O_{7.51}} \qquad \underset{\sim 950\ ^\circ C \downarrow \sim 600\ ^\circ C}{\text{tetragonal}}$$

$$\text{monoclinic}$$

Scheme 1

Table 1 Electrical conductivity of stabilized zirconia ceramics prepared by different methods

Electrolyte	Conditions of preparation	Conductivity (S cm^{-1})		Activation energy (eV)		Ref.
		800 °C	1000 °C	T < 900 °C	T > 950 °C	
$Zr_{0.92}Y_{0.08}O_{1.96}$	Co-precipitation and hot pressing (1300 °C)	2.5×10^{-2}	8.9×10^{-2}	0.84	0.46	[46]
$Zr_{0.90}Y_{0.10}O_{1.95}$		4.2×10^{-2}	1.4×10^{-1}	0.84	0.42	
$Zr_{0.92}Y_{0.08}O_{1.96}$	Co-precipitation and sintering	3.4×10^{-2}	1.4×10^{-1}	0.80	0.72	[7]
$Zr_{0.90}Y_{0.10}O_{1.95}$		2.4×10^{-2}	1.0×10^{-1}	0.80	0.72	
$Zr_{0.91}Sc_{0.09}O_{1.96}$	Co-precipitation and hot pressing (1300 °C)	1.0×10^{-1}	2.2×10^{-1}	0.79	0.38	[46]
$Zr_{0.90}Sc_{0.10}O_{1.95}$		8.9×10^{-2}	2.5×10^{-1}	0.75	0.37	
$Zr_{0.91}Sc_{0.09}O_{1.96}$	Co-precipitation and sintering	1.1×10^{-1}	3.2×10^{-1}	0.64	0.44	[7]
$Zr_{0.90}Sc_{0.10}O_{1.95}$		1.0×10^{-1}	3.0×10^{-1}	0.64	0.46	
$Zr_{0.90}Sc_{0.10}O_{1.95}$	Hot pressing (1600 °C)	8.3×10^{-2}	2.8×10^{-1}			[62]
$Zr_{0.91}Sc_{0.09}O_{1.96}$	Slip casting	1.1×10^{-1}	3.1×10^{-1}			[63]
$Zr_{0.89}Y_{0.08}Al_{0.03}O_{1.94}$	Hot pressing (1300 °C)	1.9×10^{-2}	7.9×10^{-2}			[62]
	Hot pressing (1600 °C)	5.4×10^{-2}	1.6×10^{-1}			
$Zr_{0.92}Yb_{0.08}O_{1.96}$	Co-precipitation and sintering	7.9×10^{-2}	2.2×10^{-1}	0.73	0.67	[7, 40]
$Zr_{0.90}Yb_{0.10}O_{1.95}$		5.6×10^{-2}	1.9×10^{-1}	0.72	0.63	

ZrO_2-Sc_2O_3 correlate with the transitions of the distorted fluorite phases characteristic of this system, and with thermal effects found by differential thermal analysis (DTA) [54]. A number of different theoretical models were suggested in order to explain the dependencies of the activation energy on temperature and dopant concentration (see, for instance [45, 53, 55]).

The solid electrolytes ZrO_2-Y_2O_3 and ZrO_2-Sc_2O_3, having the highest conductivity in comparison with other zirconia ceramics, were considered to be most promising electrolyte materials [2]. These materials were subjected to detailed investigations.

Phase composition, conductivity, and other properties of the ZrO_2-Y_2O_3 ceramics containing 8–12 mol% of $YO_{1.5}$ have been reported [14]. The minimum yttria concentration to stabilize the cubic fluorite phase was established to be 10 mol% . Although X-ray diffraction (XRD) of the $Zr_{0.92}Y_{0.08}O_{1.96}$ ceramics did not show the presence of phase impurities, phase heterogeneity of the material was demonstrated by optical methods. The solid solution $Zr_{0.90}Y_{0.10}O_{1.95}$, which was synthesized before ceramic sintering, exhibited the maximum conductivity [14]. Thermal expansion coefficients (TECs) of the materials are in the range of $(9.7–10.0) \times 10^{-6}$ K^{-1} (Table 2). For ZrO_2-Y_2O_3 samples prepared by hot pressing, the cubic fluorite phase stabilization was observed at a yttria content more than 6 mol% , but the conductivity maximum was found to correspond to 10 mol% of yttria [46]. At the same time, the conductivity maximum of the solid electrolytes ZrO_2-Y_2O_3 produced by thermal decomposition of organometallic compounds [45] and by hydroxide co-precipitation [7] was about 7–7.5 mol% of the stabilizing addition.

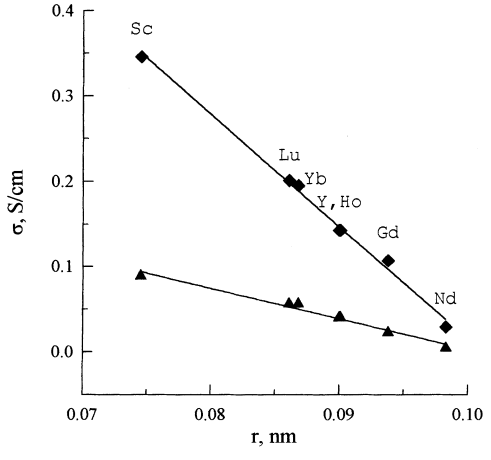

Fig. 1 Dependence of the electrical conductivity of $Zr_{0.90}R_{0.10}O_{1.95}$ ceramics (R is a rare earth element) on radii of the cations R^{3+} at 1000 °C (*1*) and 800 °C (*2*). All ceramics have been prepared by coprecipitation of hydroxides with subsequent sintering. Published data on conductivity [7, 40] have been used in this figure

Phase diagrams of the ZrO_2-Sc_2O_3 system are more complex than those of ZrO_2-Y_2O_3 [5]. In the zirconia-rich part of the ZrO_2-Sc_2O_3 system at low temperatures, there are rhombohedral β- and γ-phases ($Sc_2Zr_7O_{17}$ and $Sc_2Zr_5O_{13}$). When heated, these phases transform reversibly to the F-phase. According to the conductivity and XRD results, the reverse F $\rightarrow$ β transition proceeds according to a diffusion mechanism and the transition

Table 2 Thermal expansion coefficients (TECs) of zirconia-based ceramics

Composition	Average TEC values		Ref.
	Temperature range (°C)	$\bar{\alpha} \times 10^6$ (K^{-1})	
$Zr_{0.92}Y_{0.08}O_{1.96}$	20–850	9.8	[14]
$Zr_{0.90}Y_{0.10}O_{1.95}$	20–850	10.0	[14]
$Zr_{0.88}Y_{0.12}O_{1.94}$	20–850	9.9	[14]
$Zr_{0.85}Y_{0.15}O_{1.93}$	0–1200	10.2	[24]
$Zr_{0.50}Y_{0.50}O_{1.75}$	20–1000	9.4	[17]
$Zr_{0.83}La_{0.17}O_{1.92}$	0–1200	9.0	[24]
$Zr_{0.85}Ce_{0.15}O_{2-\delta}$	0–1200	11.5	[24]
$Zr_{0.75}Ce_{0.25}O_{2-\delta}$	0–1200	11.2	[24]
$Zr_{0.87}Sc_{0.13}O_{1.94}$	20–650	8.2	[54]
	650–900	12.7	
	900–1200	10.0	

temperatures is a function of the electrolyte processing conditions [2, 56, 57]. Such phase changes represent one of the reasons for the contradictions between data on composition dependencies of the conductivity obtained by different research groups. For instance, the maximum conductivity in the ZrO_2-Sc_2O_3 system was published to correspond to the following scandia contents (mol%): 9 [50], 9–9.5 [7], 10 [46, 47], 9–12 [48], 10–12 [51]. Fast degradation processes, analyzed below, are another important reason for the poor reproducibility of the conductivity of the ZrO_2-Sc_2O_3 ceramics.

Pyrochlores $Me_2Zr_2O_7$ (Me = La-Gd) and δ-phases $Me_4Zr_3O_{12}$ (Me = Sc, Y, Ho-Lu)

The pyrochlore phases $Me_2Zr_2O_7$ (Me = La, Nd, Sm, Gd) are characterized by existing homogeneity fields where solid solutions are formed based on them [19, 36, 43]. As an example, the solid solutions with the pyrochlore structure in the system ZrO_2-Nd_2O_3 at 1200 °C were found to exist within the range of 41 to 52–55 mol% of $NdO_{1.5}$ [31]. The concentration range of the pyrochlore solid solution formation narrows with decreasing rare-earth cation radius [14].

The pyrochlore phases possess a mixed ionic and electron hole conductivity [18, 19, 36]. The p-type conductivity was established by the EMF method and by studying oxygen partial pressure dependence of the total conductivity (the conductivity is proportional to $P_{O_2}^{1/4}$). The solid solubility of rare earth cations in the zirconium sublattice associated with the formation of the solid solution $Me_2(Zr,Me)_2O_{7-\delta}$ leads to increasing oxygen vacancy concentration and to a definite increase in both ion and electron-hole conductivity [18, 19, 36]. When the temperature increases, a transition into the fluorite phase accompanied by a sharp increase in the oxygen ionic conductivity is typical for the pyrochlores [43].

The $Ce_2Zr_2O_7$ phase was found to exist only in reducing atmospheres [21]. At the same time, solid solutions based on the $Pr_2Zr_2O_7$ pyrochlore, where praseodymium ions are predominantly in the trivalent state, are stable in air [27–29].

Physicochemical properties of the $Me_4Zr_3O_{12}$ (Me = Sc, Y, Ho-Lu) compounds have been reported [58–61]. No existence of solid solutions based on these compounds (δ-phases) was observed. When heated, the δ-phases transform to the fluorite-type solid solutions. The $\delta \rightarrow$ F transition temperature was shown to be 1370–1650 °C and to decrease with increasing rare-earth cation radius. TECs of the $Me_4Zr_3O_{12}$ ceramics are in the range $(6.5–12.2) \times 10^{-6}$ K^{-1}. The δ-phase structure represents a fluorite-based superstructure formed as a result of ordering of a part of the cation and of all the anion vacancies. Here, the anion vacancies are associated in pairs and do not take part in oxygen ion conduction. In the ordered phases, the oxygen ion transference numbers were determined to be about 0.1, whereas the transition into the disordered fluorite phase results in a dramatic increase in the ionic conductivity. The conductivity of the δ-phases increases regularly with increasing radius of the rare-earth cation.

The binary oxide systems ZrO_2-MO (M = Be, Mg, Ca, Sr, Ba)

There are no solid solutions with the fluorite structure in the ZrO_2-MO systems (M = Be, Sr, Ba) at temperatures below 1500 °C [64, 65]. The conductivity of multiphase ceramics of these systems, which contain monoclinic or tetragonal phases based on zirconia, is considerably low [64].

The ZrO_2-MgO phase diagram has been presented [66]. This system is characterized by narrow (up to 1 mol% of magnesia) range of solid solutions with monoclinic (α) and tetragonal (β) structure. An eutectoid point that corresponds to the low temperature limit of existence of the cubic fluorite was found at approximately 1300 °C and ~19 mol% MgO. The compound $Mg_2Zr_5O_{12}$, having a rhombohedral structure, was observed to form at 1750–2000 °C.

Metastable solid solutions of ZrO_2-MgO with a cubic structure were obtained and studied in numerous works (see, for example, [64, 66–68]). This system has attracted considerable attention, as the low radius of the magnesium cations gives high ionic conductivity for the materials obtained by introducing a second dopant into the ZrO_2-MgO ceramics [69]. Reducing the temperature was ascertained to lead to a decomposition of all metastable solid solutions of ZrO_2-MgO [66, 68, 70–72]. The most intensive destablization of the cubic phase was observed at 1400 °C, while the decomposition rate increases with increasing magnesia content [66, 68]. It has been also established that the ZrO_2-MgO solid solutions decompose completely under an argon atmosphere at temperature above 2000 °C owing to evaporation of the magnesia [66].

The ZrO_2-CaO solid solutions are the most stable compared to other ZrO_2-MO oxide systems and were subjected to detailed investigation. The zirconia-rich part of the ZrO_2-CaO phase diagram has been presented [73], and the thermodynamic properties of these oxide has been studied [74]. The results of EMF measurements of galvanic cells with CaF_2 as the electrolyte showed that ZrO_2-CaO cubic solid solution range extends to 17 mol% of calcia at 1200–1400 °C [74]. At temperatures below 850 °C, the saturated solid solution is thermodynamically unstable and tends to decompose to $CaZrO_3$ and ZrO_2. This is in agreement with direct experimental data, as decomposition of the ZrO_2-CaO cubic phase has also been shown [72, 73, 75–77]. The highest rate of decomposition was observed at 1200–1400 °C [66, 76]. Monoclinic zirconia and perovskite phase $CaZrO_3$ were found to be the decomposition products [72, 75]. The ZrO_2-CaO electrolytes containing 15 mol% and more calcium oxide are stable in atmospheric air and argon atmospheres at temperatures above 1000 °C [66, 76].

The crystal structure and conductivity of the ZrO_2-CaO (CSZ) solid electrolytes have been reported [64, 69, 77–80]. The ceramics at 13–15 mol% of the dopant possess maximum conductivity in the system. When the calcia content is higher than 15 mol%, an ordering of the oxygen ion sublattice results in decreasing conductivity [80]. The conductivity of the ZrO_2-CaO ceramics at temperatures above 1150 °C in the composition range from 12 to 35 mol% was observed to be essentially independent of time [77]. At lower temperatures, only the $Zr_{0.80}Ca_{0.20}O_{1.80}$ ceramics exhibit time-independent conductivity (the Zr_4CaO_9 phase is stable at medium temperatures). The resistance of the other oxide materials of the system increases with the time and is proportional to $\tau^{5/3}$, which is caused by the cubic fluorite phase decomposition.

Thus, both the stability and conductivity of CSZ is lower compared to the ZrO_2-Me_2O_3 (Me = Y, Sc) solid electrolytes. Owing to this, much of the attention of this work is concentrated on the properties of zirconia stabilized by yttria (YSZ) or by scandia (SSZ).

Solid-state synthesis and processing of the electrolyte ceramics

As both phase composition and conductivity of zirconia-based ceramics are functions of the processing conditions, numerous research projects have focused on developing technologies for the synthesis and sintering as well as on studying the kinetics of the solid-state processes [41, 81–92]. It has been stated, in particular, that it is necessary to use certain methods to prepare reactive powders in order to obtain high-quality zirconia ceramics. Methods of co-precipitation and decomposing of organometallics are among the most promising technologies [41, 44, 45, 93, 94]. Other methods were aimed at developing hot-pressing techniques [46, 56, 62, 84, 95– 98]. A brief review of the methods of processing solid electrolyte ceramics was presented by Perfilyev et al. [12].

The effect of the microstructure of the ceramic and of impurities on the properties of stabilized zirconia

As a general rule for the stabilized zirconia electrolytes, the activation energy of conductivity of the bulk of the ceramic grain is less than that of the grain boundaries [99, 100]. This results in a decreasing contribution of the grain boundaries to the total resistance with increasing temperature. When the grain size increases, the total conductivity of the polycrystalline electrolytes increases regularly owing to a decreasing boundary area [45, 100]. Therefore the grain bulk conductivity may depend on or be independent of the electrolyte processing conditions. Using hot-pressing technology allows reduction of the resistance of both the grain bulk and the boundaries [56, 101, 102]. A decrease in the boundary resistance can be also achieved by increasing the temperature of the ceramic sintering [101, 102].

It generally holds that introducing impurities into the ceramics of the completely stabilized zirconia phase leads to increasing resistance of both the grain bulk and the boundaries [101, 103]. Here, total resistance values are determined by a distribution of the impurity between the bulk and the boundaries of the ceramic grains. The effect of very soluble impurities on conductivity is less compared to poorly soluble impurities which aggregate at the grain boundary and block them. For example, small additions of manganese or iron oxides, having a high solubility in the solid cubic zirconia phase, were demonstrated to contribute to the sinterability of the ceramics and not significantly to affect the conductivity [62, 103, 104].

In some cases, one can expect a definite decrease of the grain boundary resistance with introducing dopants. An example is the uncompleted solid-state synthesis of ZrO_2-Sc_2O_3 solid electrolytes when the monoclinic phase is concentrated on the grain boundaries, which results in a relatively high resistance of the boundaries [10, 47]. In this case, a positive effect of small amounts of Fe_2O_3, Al_2O_3, Cr_2O_3, or Mn_2O_3 could be expected. These oxide additions lead to an accelerating of the solid-state reactions leading to the cubic phase formation, to decreasing the synthesis temperature, and to improving the sinterability [62, 104]. One should note also that the iron and chromium oxide additions even at concentrations of 1–2 mol% may suppress the phase transition of disordered ZrO_2-Sc_2O_3 solid solutions to rhombohedral $Zr_7Sc_2O_{17}$ [104]. A moderate doping by chromium oxide (up to 2 mol%) permits improvement of the mechanical strength and microhardness of $Zr_{0.90}Sc_{0.10}O_{1.95}$ [105], whereas iron oxide additions result in decreasing strength [62, 106].

Table 3 presents selected results of studying the resistance of grain bulk and boundaries of the zirconia polycrystalline electrolytes with different additions. Notice that different authors attained probably different impurity distributions between the grain bulk and boundaries, which is a reason for the discrepancies in the literature data.

Moderate amounts of TiO_2 (up to 0.3 mol%) were shown to dissolve uniformly in the bulk of the grain of ZrO_2-Y_2O_3 and ZrO_2-Sc_2O_3, which leads to increasing density and mechanical strength of the ceramics [63]. Additions up to 3 mol% Al_2O_3 distribute into both the grain bulk and the grain boundaries of the zirconia materials and provides an increase in thermal shock resistance. At the same time, both doping types lead to an increase in the electrical resistance of the electrolytes.

The sinterability of stabilized zirconia was found to be enhanced on introduction of bismuth oxide into the ceramic [62, 107, 108]. Moreover, bismuth oxide additions do not significant alter the electrical resistance. The solid solubility of bismuth oxide in zirconia is very low, but most of the bismuth oxide evaporates during the

Table 3 Effect of additions on the electrical properties of stabilized zirconia[a]

Electrolyte	Measurement temperature (°C)	Addition (mol%)	ρ_b (Ω cm)	ρ_{gb} (Ω cm)	ρ/ρ_b (%)	Ref.
$Zr_{0.91}Y_{0.09}O_{1.96}$	500	–	1010	70	107	[101]
		1.0 $FeO_{1.5}$	1610	320	120	
		1.0 MgO	1370	380	128	
		1.0 TiO_2	1120	130	112	
		1.0 $AlO_{1.5}$	1250	150	112	
$Zr_{0.91}Y_{0.09}O_{1.96}$	450	–	2340	140	106	[101]
		0.5 MgO	4180	280	107	
		1.0 MgO	4880	8000	116	
		5.0 MgO	9620	3540	137	
		3.0 SiO_2	4810	1400	129	
$Zr_{0.91}Sc_{0.09}O_{1.96}$	500	–	456	32	107	[63]
		0.1 TiO_2	477	52	111	
		0.1 $AlO_{1.5}$	483	41	108	
		0.1 $AlO_{1.5}$	742	38	105	
		3.0 $AlO_{1.5}$	854	57	107	
$Zr_{0.91}Sc_{0.09}O_{1.96}$	450	–	1330	260	120	[103]
		0.1 $FeO_{1.5}$	1290	240	119	
		1.0 $FeO_{1.5}$	1570	250	116	

[a] ρ_b, ρ_{gb}, and ρ are the resistance of the grain bulk, of the grain boundary, and the total resistance of the ceramics, respectively

sintering [107]. As a result, the mixtures of zirconia and bismuth oxide were a single phase after sintering [107]. However, hot processing of the solid electrolytes $Zr_{0.89}Y_{0.08}Al_{0.03}O_{1.94}$ and $Zr_{0.90}Sc_{0.10}O_{1.95}$ with additions of bismuth oxide was observed to result in the formation of metallic bismuth-embedded particles [62].

Additions of Ta_2O_5, Nb_2O_5, V_2O_5, and WO_3 were observed to lead to a destabilizing of the cubic zirconia phase and to dramatically decrease the conductivity [104, 108]. This is caused by the formation of compounds of these oxides with rare-earth oxide dopants [108–110]. In particular, the formation of rare-earth element tantalates and an acceleration of the decomposition of the cubic phase were noted when Ta_2O_5 was added to the electrolytes of the ZrO_2-Me_2O_3 systems (Me = Nd, Sm, Dy, Y) [109]. Analogously, introducing Ta_2O_5 into either the $Zr_{0.90}Sc_{0.10}O_{1.95}$ electrolyte synthesized earlier, or into the starting mixture of zirconia and yttria, has led to a destabilizing of the cubic fluorite structure with formation of tetragonal zirconia [110], which is caused by the formation of $YTaO_4$. The conductivity of the $Zr_{0.90}Sc_{0.10}O_{1.95}$-$Ta_2O_5$ ceramics decreases sharply with an increasing content of tantalum oxide, but it is predominantly ionic at additions up to 15 mol% of tantalum oxide. The results of incorporation of Nb_2O_5 and V_2O_5 into the electrolyte $Zr_{0.90}Sc_{0.10}O_{1.95}$ are analogous: decomposition of the cubic phase and decreasing conductivity, while the ionic character of the conductivity is maintained [108, 110].

Adding LiF and AlF_3 fluorides allowed reduction of the temperature of hot pressing of the solid electrolytes $Zr_{0.89}Y_{0.08}Al_{0.03}O_{0.194}$ and $Zr_{0.90}Sc_{0.10}O_{1.95}$ as well as resulting in increasing ceramic density [62]. However, these additions decrease the conductivity and destabilize the cubic zirconia phase. Doping with GeO_2 and B_2O_3 may improve the sinterability [86], but one can expect an increasing resistance of the ceramic grain boundaries in this case.

Time degradation of conductivity

The decreasing conductivity of zirconia solid electrolytes with time is determined by the following factors: (1) decomposition of a metastable solid solution at reduced temperatures; (2) local ordering of the oxygen sublattice of completely stabilized electrolytes with formation of microdomains; (3) changing resistance of the ceramic gain boundaries; (4) interaction between electrochemical cell materials [2, 111].

The decomposition of metastable cubic phases is characteristic of the electrolytes ZrO_2-Y_2O_3 and ZrO_2-Sc_2O_3 containing less than 9 mol% of $MeO_{1.5}$ [66, 111, 112] as well as of ZrO_2-CaO ceramics [16, 66, 76, 77]. The degradation of such electrolytes is accompanied by two process: the increasing concentration of new centers of phase formation and their growth [111, 112]. For a sufficiently long time of annealing, the first process comes to an end. Under the assumption that the conductivity of the starting phase is significantly higher than that of the product phase, the following equations were proposed in order to describe the degradation kinetics [111, 112]:

$$\sigma_\tau = \sigma_0(1 - A \cdot \tau) \text{ for long periods} \quad (1)$$

$$\sigma_\tau = \sigma_0(1 - B \cdot \tau^{5/3}) \text{ for short periods} \quad (2)$$

where σ_0 and σ_τ are the specific electrical conductivities at the start and at the time τ, respectively; A and B are constants. The time dependence of the conductivity of the metastable electrolytes YSZ, SSZ, and CSZ can be described adequately by Eq. 2 for periods up to 400 [77, 112].

The decomposition of the metastable solid solutions is characterized by an increasing activation energy for electrical conductivity with time and by a decreasing maximum degradation degree (so called degradation depth) with increasing temperature [111]. At higher temperatures, when the cubic phase is thermodynamically stable, there is no degradation in the behavior of such materials [111].

The formation of microdomains with the ordered oxygen sublattice, which causes a decrease in conductivity with time, occurs for the single-phase solid electrolytes at low temperatures [111, 113, 114]. The decrease in conductivity was demonstrated to be reversible, not to depend on a degradation process, and to take place at temperature below a well-defined characteristic temperature [114]. For the ZrO_2-Y_2O_3 electrolytes the characteristic temperature of the start of the degradation is 1030–1200 °C, whereas this temperature for single crystals of $Zr_{0.90}Y_{0.10}O_{1.95}$ is about 1000 °C [111, 114]. The activation energy for electrical conductivity increases with the degradation [113]. Composition dependences of the degradation depth exhibit a maximum. In the ZrO_2-Y_2O_3 system, such a maximum was observed to be at 15–25 mol% of yttria and it is shifted to lower yttria concentrations with decreasing temperature [114]. Therefore the degradation rate is a function of temperature and stabilizing dopant content.

The grain boundary resistance may provide either a positive or negative contribution to the conductivity degradation process [101, 114, 115]. As a particular case, introducing magnesia into YSZ leads to an increasing resistance of the grain boundary with time [115].

One should note that the time degradation is a reason for numerous disagreements between literature data on the conductivity of the electrolytes, as well as for some anomalies in their behavior such as a dramatic increase in conductivity of the ZrO_2-Y_2O_3 ceramics with increasing temperature [111, 116].

Selected data on the time degradation of the zirconia electrolytes are given in Table 4. The degradation rate of the ZrO_2-Sc_2O_3 and ZrO_2-CaO ceramics is significantly higher than that of YSZ [111, 115, 117]. With regard to this, of interest are results concerning the solid electrolytes of ZrO_2-Sc_2O_3-Y_2O_3 [45]. These materials exhibit a higher conductivity than with YSZ and a much lower rate of degradation than SSZ. So, if the conduc-

Table 4 Time degradation of the conductivity of stabilized zirconia ceramics[a]

Electrolyte	Measurement temperature (°C)	Time and conditions of annealing	$\Delta\rho/\rho$ (%)	$\Delta\rho_b/\rho_b$ (%)	$\Delta\rho_{gb}/\rho_{gb}$ (%)	Ref.
$Zr_{0.90}Y_{0.10}O_{1.95}$	1000	2600 h, 1000 °C, air/H_2 gradient	−5	–	–	[117]
	1000	2600 h, 1000 °C, H_2	10	–	–	
	1000	4300 h, 1000 °C, air	−17	–	–	
	1100	4700 h, 1100 °C, air	8	–	–	
$Zr_{0.93}Y_{0.07}O_{1.97}$	500	430 h, 1100 °C, air	88	84	30	[111]
$Zr_{0.90}Y_{0.10}O_{1.95}$	500	430 h, 1100 °C, air	4	1	18	[111]
$Zr_{0.92}Y_{0.03}O_{1.96}$	450	320 h, 830 °C, O_2	18	15	90	[101]
	500		20	19	31	
$Zr_{0.88}Y_{0.12}O_{1.94}$	450	320 h, 830 °C, O_2	8	8	12	[101]
	500		13	14	4	
$Zr_{0.90}Y_{0.10}O_{1.95}$	1000	100 h, 1000 °C, air	1	–	–	[113]
$Zr_{0.867}Y_{0.133}O_{1.933}$			4	–	–	
$Zr_{0.85}Y_{0.15}O_{1.92}$			10	–	–	
$Zr_{0.90}Y_{0.10}O_{1.95}$ (single crystal)	880	1000 h, 880 °C, air	5	–	–	[113]
	725	1000 h, 725 °C, air	24	–	–	
$Zr_{0.91}Y_{0.09}O_{1.96}$ + 0.5% MgO	450	100 h, 830 °C, O_2 +	10	5	24	[115]
$Zr_{0.91}Sc_{0.09}O_{1.96}$	450	120 h, 830 °C, CO	52	59	12	[115]
$Zr_{0.91}Sc_{0.09}O_{1.96}$	900	300 h, 900 °C, air	40	–	–	[45]
$Zr_{0.905}Sc_{0.095}O_{1.952}$	500	430 h, 1100 °C, air	41	46	17	[111]
$Zr_{0.90}Sc_{0.10}O_{1.95}$	500	430 h, 1100 °C, air	55	95	−67	[111]
$Zr_{0.90}Sc_{0.10}O_{1.95}$	1000	2500 h, 1000 °C, air	50	–	–	[117]
	1100	4700 h, 1100 °C, air	41	–	–	
$Zr_{0.90}Y_{0.04}Sc_{0.06}O_{1.95}$	900	300 h, 900 °C, air	0	–	–	[45]
$Zr_{0.90}Y_{0.03}Sc_{0.07}O_{1.95}$			3	–	–	
$Zr_{0.92}Y_{0.05}Sc_{0.03}O_{1.96}$			2	–	–	
$Zr_{0.90}Y_{0.04}Sc_{0.06}O_{1.95}$	500	430 h, 1100 °C, air	−2	−0.5	−10	[111]
$Zr_{0.87}Ca_{0.13}O_{1.87}$	1000	2500 h, 1000 °C, air	82	–	–	[117]
	1100	4700 h, 1100 °C, air	80	–	–	
$Zr_{0.88}Ca_{0.12}O_{1.88}$	1200	100 h, 1200 °C, air	64	–	–	[77]
$Zr_{0.85}Ca_{0.15}O_{1.85}$	1200		30	–	–	

[a] $\Delta\rho/\rho$ is the ratio between the increase of total resistance after annealing and the starting value of the resistance; $\Delta\rho_b/\rho_b$ and $\Delta\rho_{gb}/\rho_{gb}$ are the same quantities for the resistance of the grain bulk and grain boundary, respectively

tivity at temperatures of 650–1000 °C before degradation was observed to decrease in the sequence $Zr_{0.905}Sc_{0.095}O_{1.952} > Zr_{0.90}Y_{0.04}Sc_{0.06}O_{1.95} > Zr_{0.93}Y_{0.07}O_{1.97} > Zr_{0.90}Y_{0.10}O_{1.95}$, the conductivity after annealing at 1020 °C for 650 h follows the relation $Zr_{0.90}Y_{0.04}Sc_{0.06}O_{1.95} > Zr_{0.905}Sc_{0.095}O_{1.952} > Zr_{0.90}Y_{0.10}O_{1.95} > Zr_{0.93}Y_{0.07}O_{1.97}$ [111]. However, a definite degradation in conductivity with time is typical for the $Zr_{0.90}Y_{0.04}Sc_{0.06}O_{1.95}$ electrolyte also [111].

The authors [117] demonstrated that diffusion of nickel and cobalt into the bulk of stabilized zirconia at 900–1100 °C for 10 000 h did not result in a degradation of the electrolytes. It was also shown that a direct current through a solid electrolyte may lead to redistribution of the stabilizing dopant in the bulk of the electrolyte [118].

Electrolytes of ternary oxide systems

Studies of ternary oxide systems on based on zirconia were often associated with attempts to improve the properties of the electrolytes of binary systems, such as to increase the conductivity, to suppress the degradation, or to reduce costs. One of the most successful attempts [45] concerned the solid solutions of ZrO_2-Sc_2O_3-Y_2O_3. Materials containing 3–7 mol% of $YO_{1.5}$ and up to 6 mol% $ScO_{1.5}$ were ascertained to combine the best properties of the systems ZrO_2-Sc_2O_3 and ZrO_2-Y_2O_3, which exhibit high conductivity and negligible degradation [45]. Construction of 'property versus composition' diagrams using the simplex method [119] confirmed afterwards the initial conclusions [45] concerning the most promising compositions of the system ZrO_2-Sc_2O_3-Y_2O_3. High-conductivity electrolytes were also found in the system ZrO_2-Yb_2O_3-Y_2O_3 [120].

Common typical features of known zirconia-based ternary systems are as follows.

1. There are no new ternary phases in the zirconia-rich part. The cubic fluorite phase stabilization is observed only in such ternary systems where the F-phase exists in binary system.
2. Limited solid solubility of the third component in binary oxide compounds typically takes place. The solid solubility of oxides which do not stabilize the F-phase in the binary oxide systems is extremely low.
3. The features of the composition dependences of the conductivity in ternary systems coincide with those typical for the binary systems. Therefore conductivity values of the ternary cubic solid solutions are intermediate between the values of the binary solid solutions. In particular, the conductivity is at a maximum when the dopant concentration is close to low stabilization limit, and decreases with further additions of the dopants.

The discussed features are typical, for instance, for the systems ZrO_2-Sc_2O_3-CaO [121], ZrO_2-Y_2O_3-CaO [122, 123], ZrO_2-Y_2O_3-MgO [124], ZrO_2-Y_2O_3-Al_2O_3 [108], ZrO_2-CaO-MgO [69, 125], and ZrO_2-CaO-Al_2O_3 [126–128]. As an example, the formation of a ternary solid solution was not observed in the ZrO_2-SrO-CaO, system and substituting calcium by strontium oxide results in destabilizing the cubic phase [129]. One can also refer to published phase diagrams and data on selected phase relationships for the systems ZrO_2-Al_2O_3-MgO [130], ZrO_2-Al_2O_3-SrO [131], ZrO_2-Al_2O_3-BaO [132, 133], and ZrO_2-Al_2O_3-Nd_2O_3 [134].

A segment of the ZrO_2-Y_2O_3-Al_2O_3 phase diagram has been studied [108]. The solid solubility of aluminium oxide in the ZrO_2-Y_2O_3 cubic phase was found to be approximately 4 mol%. The maximum conductivity observed in the ZrO_2-Y_2O_3-Al_2O_3 system did not exceed the conductivity of the binary solid solutions of ZrO_2-Y_2O_3 containing 8–10 mol% of yttria. The aluminia additions contribute to the sinterability of zirconia ceramics as well as improving the mechanical strength.

A subsolidus phase diagram of ZrO_2-HfO_2-CaO has been presented [135]. It was established that zirconium cations in the cubic fluorite-type solid solutions of $(Zr_{1-x}Hf_xO_2)$-CaO can be substituted by hafnium cations within the entire concentration range ($0 \leq x \leq 1$). The cubic unit cell parameter decreases with increasing hafnia content [135]. Analogous results were obtained for the $(Zr_{0.70}Hf_{0.30}O_2)$-CaO cross-section [136].

Finally, one may also refer to research on conductivity, phase conductivity, and stability of the solid solutions of ZrO_2-Y_2O_3-MgO-CaO [137]. $Zr_{0.87}Ca_{0.02}Mg_{0.07}Y_{0.04}O_{1.89}$ was suggested to exhibit the most favourable properties in this system.

Mixed conductors of zirconia stabilized by rare earth oxides

The presence of significant electronic conductivity is characteristic for materials of the binary and ternary oxide systems based on zirconia containing ceria or praseodimia. As a rule, electron transference numbers of the fluorite solid solutions of this type do not exceed 0.1.

In the ZrO_2-CeO_2 system, the F-phase was found to form at temperatures above 1500 °C in the range 15–25 mol% of ceria [24]. At 1200 °C, decomposition of these solid solutions leads to formation of ceria and zirconia mixtures [24]. Incorporation of a second rare-earth oxide dopant permits stabilization of the F-phase at low temperatures. There is information on the solid solutions of ZrO_2-Y_2O_3-CeO_2 having significant electronic conductivity with predominant ionic conductivity [138]. Analogously to the solid solutions of binary systems, the $Zr_{0.85}Ce_{0.12}Y_{0.03}O_{2-\delta}$ power prepared by co-operation was a single phase after annealing even at 400 °C [139].

Moderate electronic conductivity was mentioned for the ZrO_2-Y_2O_3-Nd_2O_3 ceramics [138]. In this system the electronic conductivity is essentially smaller than that of ZrO_2-Y_2O_3-CeO_2 and it is proportional to the concentration of neodymium oxide.

In the case of cubic solid solutions of ZrO_2-Pr_6O_{11}, the electronic conductivity increases with praseodymia additions, but the oxygen ion transference numbers measured were higher than 0.9 [27, 28, 29]. Poor ceramic properties for materials of this system were noted.

Mixed conductors of stabilized ZrO_2 doped with transition metal oxides

The results of studying mixed conductors based on zirconia doped with transition metal oxides have been published [105, 107, 108, 110, 140–148]. For these materials, common typical features may be defined as follows.

1. No new phases with mixed conductivity in the zirconia-rich parts of the binary and ternary systems including zirconia, a transition metal oxide, and a stabilizing oxide dopant were observed.
2. The solid solubility of the transition metal oxides in the fluorite lattice is typically low.
3. As a general rule, introducing small additions of the transition metal oxides within the solid solubility limits results in decreasing total conductivity and maintenance of its ionic nature. Further doping leads to a separation of a transition metal oxide phase and is accompanied with a further decrease in ionic conductivity and an increase in electronic conductivity, especially at low temperatures.
4. Increasing solid solubility of the transition metal cations with increasing temperature is characteristic of most studied ternary systems. This is the reason for the reporting of different data on the phase composition, which was usually studied at room temperature.
5. The phase separation of a transition metal oxide starts at the ceramic grain boundaries. Later, the second phase forms grains and cross-linked structures, and the conductivity approaches that of the pure transition metal oxide.
6. When the concentration of the stabilizing dopant is changed, variations in the ionic conductivity of the ceramics are analogous to those of the binary systems without the addition of transition metals.

Table 5 presents data on phase composition, electrical conductivity, and oxygen ion transference numbers of some mixed conductors based on stabilized zirconia. The phase composition was determined by both XRD and petrographic methods. The ion transference numbers were measured by the EMF method using electrochemical cells where the oxygen partial pressure at the electrodes was kept at 1.0 and 0.21 bar. The oxygen ion transference numbers (t_0) were estimated by the relationship

Table 5 Electrical properties of zirconia ceramics doped by transition metal oxides[a]

Chemical composition	Phase composition	Total electrical conductivity (S cm^{-1})		Ion transference number		Ref.
		1000 °C	700 °C	1000 °C	700 °C	
$Zr_{0.855}Y_{0.100}Ti_{0.045}O_{2-\delta}$	F	4.6×10^{-2}	5.2×10^{-3}	0.96	0.97	[140]
$Zr_{0.81}Y_{0.10}Ti_{0.09}O_{2-\delta}$	F	3.0×10^{-2}	2.6×10^{-3}	0.98	0.97	[140]
$Zr_{0.72}Y_{0.10}Ti_{0.18}O_{2-\delta}$	F′	8.3×10^{-3}	5.5×10^{-4}	0.60	0.93	[140]
$Zr_{0.90}Sc_{0.08}Cr_{0.02}O_{2-\delta}$	F	1.2×10^{-1}	1.1×10^{-2}	0.99	0.97	[142]
$Zr_{0.90}Y_{0.08}Cr_{0.02}O_{2-\delta}$	F	1.3×10^{-1}	1.1×10^{-2}	0.99	0.98	[142]
$Zr_{0.90}Y_{0.08}Mn_{0.02}O_{2-\delta}$	F	8.1×10^{-2}	5.1×10^{-3}	1.00	0.96	[144]
$(Zr_{0.90}Y_{0.10}O_{1.95})_{0.96}(MnO_{1.33})_{0.04}$	F	7.0×10^{-3}	2.0×10^{-3}	1.00	0.97	[143]
$(Zr_{0.90}Y_{0.10}O_{1.95})_{0.901}(MnO_{1.33})_{0.099}$	F + Mn	1.1×10^{-1}	1.5×10^{-2}	0.63	–	[143]
$(Zr_{0.90}Y_{0.10}O_{1.95})_{0.95}(FeO_{1.5})_{0.05}$	F	3.9×10^{-2}	2.9×10^{-3}	0.99	0.88	[143]
$(Zr_{0.90}Y_{0.10}O_{1.95})_{0.90}(FeO_{1.5})_{0.10}$	F	3.6×10^{-2}	6.6×10^{-3}	0.53	0.04	[143]
$(Zr_{0.90}Y_{0.10}O_{1.95})_{0.85}(FeO_{1.5})_{0.15}$	F + Fe	3.4×10^{-2}	1.2×10^{-2}	0.22	0.01	[143]
$Zr_{0.92}Sc_{0.06}Fe_{0.02}O_{2-\delta}$	F	1.6×10^{-1}	1.4×10^{-2}	1.00	0.99	[145]
$Zr_{0.90}Sc_{0.08}Fe_{0.02}O_{2-\delta}$	F′	2.0×10^{-1}	2.0×10^{-2}	0.98	0.99	[145]
$Zr_{0.90}Sc_{0.07}Fe_{0.03}O_{2-\delta}$	F′	2.0×10^{-1}	1.9×10^{-2}	0.99	0.98	[145]
$Zr_{0.90}Sc_{0.05}Fe_{0.05}O_{2-\delta}$	F + M + Fe	2.8×10^{-2}	1.8×10^{-3}	0.97	0.97	[145]
$Zr_{0.85}Sc_{0.10}Fe_{0.05}O_{2-\delta}$	F	2.9×10^{-1}	8.9×10^{-3}	1.00	0.99	[145]
$Zr_{0.85}Sc_{0.08}Fe_{0.07}O_{2-\delta}$	F + Fe	3.2×10^{-1}	1.1×10^{-2}	1.00	1.00	[145]
$(Zr_{0.85}Ca_{0.15}O_{1.85})_{0.942}(FeO_{1.5})_{0.058}$	F	1.9×10^{-2}	7.4×10^{-4}	1.00	0.93	[146]
$(Zr_{0.85}Ca_{0.15}O_{1.85})_{0.905}(FeO_{1.5})_{0.095}$	F	2.8×10^{-2}	2.1×10^{-3}	0.72	0.15	[146]
$(Zr_{0.85}Ca_{0.15}O_{1.85})_{0.70}(NiO)_{0.30}$	F + Ni	9.9×10^{-3}	2.5×10^{-4}	1.00	0.99	[146]
$(Zr_{0.85}Ca_{0.15}O_{1.85})_{0.50}(NiO)_{0.50}$	F + Ni	9.8×10^{-3}	6.3×10^{-4}	0.42	0.08	[146]
$(Zr_{0.90}Y_{0.10}O_{1.95})_{0.90}(CuO)_{0.10}$	F + Cu	–	3.6×10^{-3}	–	0.42	[107]
$(Zr_{0.90}Y_{0.10}O_{1.95})_{0.85}(CuO)_{0.15}$	F + Cu	–	2.4×10^{-3}	–	<0.05	[107]

[a] F is the fluorite-type cubic phase; F′ is the fluorite-type phase with rhombohedral distortions; M is the monoclinic phase of zirconia; Mn corresponds to the manganese oxide phase $MnO_{1.33}$; Fe corresponds to the iron oxide phase $FeO_{1.5}$; Ni corresponds to the nickel oxide phase NiO; Cu corresponds to the copper oxide phase CuO

$$t_0 = \frac{E}{E_{\text{theor}}} = \frac{E}{(RT/4F) \cdot \ln[p_2/p_1]} \quad (3)$$

where E and E_{theor} are the values of measured and theoretical EMF, respectively, and p_1 and p_2 are the partial oxygen pressures at the electrodes. Notice that Gorelov [149] later showed a possible underestimation of the transference numbers determined by this method, caused by the polarization resistance of the electrodes.

The ternary systems ZrO_2-Me_2O_3-$M'O_x$(Me = Y of Sc; M′ = Ti, Cr, or Mn)

Titania is the transition metal oxide having the highest solid-solubility in the stabilized zirconia lattice. So the concentration range forming solid solutions of $Zr_{1-x-y}Y_xTi_yO_{2-\delta}$ ($x = 0.10$–0.20) corresponds to y values from 0 to about 0.18 [140]. Further increase in the titania content leads to the formation of the compounds $Y_2Ti_2O_7$ and $ZrTiO_4$ along with the fluorite phase. The electrical conductivity of the solid solutions was observed to decrease with y while the yttria content is constant, and the electronic conductivity increases with titania additions [140]. In the $Zr_{0.85-y}Mg_{0.15}Ti_yO_{2-\delta}$ ($y = 0$–0.85) system, single-phase fluorites were not found, and the conductivity of the ternary oxides is relatively low and of mixed ionic-electronic nature [140].

According to the results of studying the phase diagram of ZrO_2-Cr_2O_3 [148], there are no compounds in this system. In the system, only solid solutions of zirconia in chromium oxide were established [148]. The solid solubility of chromia in the electrolytes ZrO_2-Y_2O_3 and ZrO_2-Sc_2O_3 is relatively low (2–3 mol%) [141]. The addition of even 1 mol% of chromium oxide was noted to result in a transition of the rhombohedrally distorted fluorite-like phase of $Zr_{0.90}Sc_{0.10}O_{1.95}$ into a cubic one. A significant increase of the solid solubility of chromia in the system ZrO_2-Y_2O_3 with increasing temperature was mentioned. Within the solubility limits (up to 3 mol% of chromia) the conductivity decreases and is predominantly ionic [142]. Further doping with chromia leads to increasing electronic conductivity. Therefore the chromium oxide phase distributes firstly at the grain boundaries of the zirconia ceramics [142].

The solid solubility limit of manganese oxide in the fluorite phase $Zr_{0.90}Y_{0.10}O_{1.95}$ is about 5–6 mol% [143]. Doping with manganese oxide was demonstrated to lead to a decrease in the ionic conductivity, whereas significant electronic conductivity can be detected only at a $MnO_{1.33}$ content higher than 10 mol% . The activation energy for electronic conductivity is essentially lower than that for ionic conductivity. As a result, oxygen ion transference numbers increase with temperature.

It was reported [108] that incorporation of small amounts of manganese or iron oxides into the near-cathode layers of stabilized zirconia electrolytes may reduce the polarization of SOFC cathodes.

Iron-doped stabilized zirconia

In the system ZrO_2-Fe_2O_3 at iron oxide concentrations up to 50 mol% , co-existing phases of monoclinic zirconia and iron oxide were detected [108, 143]. There is weak solid solubility of iron oxide in the monoclinic zirconia phase. The stabilization of the cubic fluorite phase by a second dopant results in a sharp increase of the solid solubility of iron oxide [143].

As a consequence of the temperature dependence of the solid solubility of iron oxide in the fluorite lattice, literature data are contradictory on the concentration range for the formation of an iron-containing cubic solid solution. The maximum solubility of iron oxide was found to be 10–15 mol% for the electrolyte $Zr_{0.90}$-$Y_{0.10}O_{1.95}$ [108, 143], 5–6 mol% for the system ZrO_2-Sc_2O_3-Fe_2O_3 [145], and 8–10 mol% for $Zr_{0.85}$ $Ca_{0.15}$-Fe_2O_3 [146]. For all these systems the iron cations incorporate into zirconium lattice sites and doping by iron leads to decreasing ionic conductivity. Kotlyar et al. [108, 143] attributed the decrease of the ionic conductivity to the formation of defect associates between oxygen ion vacancies and iron cations. The conductivity of the ceramics containing up to 5 mol% of iron oxide is predominantly ionic. When the iron oxide content is higher than 5–6 mol% , an increase of the electronic conductivity is detected. Therefore the contribution of the electronic component to the total conductivity increases with decreasing temperature owing to a lower activation energy for electronic conduction in comparison to the ionic one. Decreasing yttria additions to the solid solutions of ZrO_2-Y_2O_3-Fe_2O_3 leads to a regular increase in ionic conductivity [108].

Studies of the mixed conductors ZrO_2-Y_2O_3-Fe_2O_3 by thermogravimetric analysis (TGA) and electron paramagnetic resonance (EPR) showed that iron cations predominantly exist in the stabilized zirconia in bivalent and trivalent states [108]. The electronic transport occurs electron hopping between iron cations.

The incorporation of iron oxide into zirconia-based ceramics was found to improve the sinterability, to increase the solid-state reaction rate, and to decrease the temperature necessary for the stabilization of zirconia synthesized by the standard ceramic technology [83, 145].

Doping zirconia by cobalt, nickel, and copper oxides

A low solid solubility in stabilized zirconia is characteristic of the oxides of cobalt, nickel, and copper. Thus, the solubility limit of cobalt oxide in YSZ was found not to exceed 3 mol% of $CoO_{1.33}$ [143]. Studies by the XRD and petrographic methods did not detect the cobalt oxide phase when additions of $CoO_{1.33}$ into $Zr_{0.90}Y_{0.10}$-$O_{1.95}$ were less than 8 mol% and the solubility limit was estimated from independence of the fluorite unit cell parameter on the cobalt oxide content [143]. The conductivity of YSZ decreases upon doping with moderate

cobalt oxide amounts (up to 10 mol%) and it is predominantly ionic within this concentration range. Further doping leads to a considerable increase of the electronic conductivity of the ceramic materials.

The solid solubility of nickel oxide in the $Zr_{0.90}Y_{0.10}O_{1.95}$ and $Zr_{0.85}Ca_{0.15}O_{1.85}$ electrolytes is extremely low (less than 2 mol% of NiO) [67, 143, 146]. The electrical conductivity of the ceramics decreases monotonically with doping by nickel oxide and is predominantly ionic up to 30 mol% of NiO in the temperature range 600–1100 °C. In the case that the nickel oxide content exceeds 30 mol%, the electronic conductivity increases with further addition.

The maximum solubility of copper oxide in the fluorite phase $Zr_{0.90}Y_{0.10}O_{1.95}$ was less than 5 mol% [107]. Introducing larger quantities of copper oxide results in formation of CuO (Cu_2O) as a separate phase, which distributes predominantly at the ceramic grain boundaries and forms continuous electron-conducting bridges at high concentrations. Both the fluorite unit cell parameter and the conductivity decrease upon incorporation of copper cations into the crystal lattice of the solid solution of $Zr_{0.90}Y_{0.10}O_{1.95}$- CuO. The phase segregation of copper oxide exhibits no effect on the resistance of the ceramics at high temperatures but increases the electronic conductivity at temperatures below 600 °C. The conductivity of the two-phase ceramic materials containing more than 10 mol% of CuO is mixed ionic-electronic. For such materials, oxygen ion transference numbers were found not to exceed 0.5.

Oxygen permeability of stabilized zirconia ceramics

The electrolytic domain where electronic conductivity and oxygen permeability are negligible is one of the key features of oxygen-conducting solid electrolytes determining their applicability [1–3]. In contrast, development of oxygen-separation membranes requires maximum values of both the ionic and electronic partial conductivities. Therefore, publications concerning the electronic transport in zirconia-based ceramics are of special interest.

Theoretical questions of oxygen permeation through stabilized zirconia solid electrolytes were analysed in detail by Vecher et al. [150–154]. It was shown, in particular, that one has to take into consideration the electronic conductivity of the electrolytes when applying them for thermodynamic studies and for the analysis of media with low oxygen partial pressures. A number of empirical and theoretical methods to estimate electronic transport parameters in zirconia-based materials were proposed [150].

Gilderman et al. [104, 155–157] have studied the oxygen permeability of the solid electrolytes $Zr_{0.90}Y_{0.10}O_{1.95}$, $Zr_{0.89}Y_{0.08}Al_{0.03}O_{1.95}$, $Zr_{0.85}Ca_{0.15}O_{1.85}$, and $Zr_{0.90}Sc_{0.10}O_{1.95}$ in the temperature range 900– 1240 °C at oxygen partial pressures of 0.01–1 atm. Under such conditions, the oxygen transport through zirconia ceramics was demonstrated to be limited by p-type electronic conductivity. Within the studied range of temperature and oxygen pressure, the flux density of oxygen permeation j_{O_2} ($cm^3\ cm^{-2}\ s^{-1}$) can be described by the following equations:

$$j_{O_2} = 1.55 \exp\left(-\frac{43.1 \pm 0.3\ \text{kcal mol}^{-1}}{RT}\right) \times \frac{p_2^{1/4} - p_1^{1/4}}{d} \quad \text{for } Zr_{0.90}Y_{0.10}O_{1.95} \tag{4}$$

$$j_{O_2} = 1.52 \exp\left(-\frac{42.7 \pm 0.5\ \text{kcal mol}^{-1}}{RT}\right) \times \frac{p_2^{1/4} - p_1^{1/4}}{d} \quad \text{for } Zr_{0.89}Y_{0.08}Al_{0.03}O_{1.95} \tag{5}$$

$$j_{O_2} = 1.93 \times 10^{-1} \exp\left(-\frac{38.9 \pm 0.6\ \text{kcal mol}^{-1}}{RT}\right) \times \frac{p_2^{1/4} - p_1^{1/4}}{d} \quad \text{for } Zr_{0.90}Sc_{0.10}O_{1.95} \tag{6}$$

$$j_{O_2} = 3.82 \times 10^{-1} \exp\left(-\frac{37.2 \pm 0.4\ \text{kcal mol}^{-1}}{RT}\right) \times \frac{p_2^{1/4} - p_1^{1/4}}{d} \quad \text{for } Zr_{0.85}Ca_{0.15}O_{1.85} \tag{7}$$

where d (cm) is the thickness of the cermics, and p_1 and p_2 (atm) are the values of the oxygen partial pressure at the membrane permeate side and feed side, respectively. The oxygen permeability of the ceramics decreases in the sequence $Zr_{0.85}Ca_{0.15}O_{1.95} > Zr_{0.89}Y_{0.08}\ Al_{0.03}O_{0.195} > Zr_{0.90}Y_{0.10}O_{1.95} > Zr_{0.90}Sc_{0.10}O_{1.95}$ (Fig. 2). The electron-hole transference numbers decrease in an analogous way from 5×10^{-5} ($Zr_{0.90}Sc_{0.10}O_{1.95}$) to 1×10^{-3}

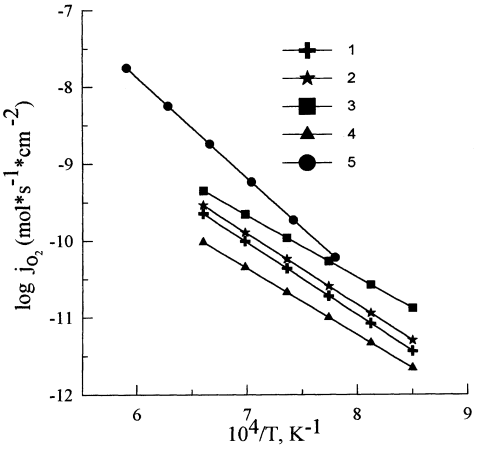

Fig. 2 Temperature dependence of the flux density of oxygen permeation through solid electrolyte ceramics: *1* $Zr_{0.90}Y_{0.10}O_{1.95}$ [155], *2* $Zr_{0.89}Y_{0.08}Al_{0.03}O_{1.95}$ [157], *3* $Zr_{0.85}Ca_{0.15}O_{1.85}$ [157], *4* $Zr_{0.90}Sc_{0.10}O_{1.95}$ [157], *5* $Zr_{0.85}Ca_{0.15}O_{1.85}$ [158] at an oxygen partial pressure gradient of 0.21 atm/1.3× 10^{-4} atm. The thickness of the electrolyte membranes is 1 mm

($Zr_{0.85}Ca_{0.15}O_{1.85}$). The characteristic oxygen pressures P_h (atm), corresponding to equal p-type electronic and ionic conductivities, were calculated from the data on oxygen permeation to be

$$P_h^{1/4} = 5.12 \times 10^{-4}\, T \exp\left[\frac{20.0\,\text{kcal mol}^{-1}}{RT}\right]$$
for $Zr_{0.90}Sc_{0.10}O_{1.95}$ (8)

$$P_h^{1/4} = 1.25 \times 10^{-3}\, T \exp\left[\frac{22.9\,\text{kcal mol}^{-1}}{RT}\right]$$
for $Zr_{0.90}Y_{0.10}O_{1.95}$ (9)

$$P_h^{1/4} = 1.61 \times 10^{-3}\, T \exp\left[\frac{21.1\,\text{kcal mol}^{-1}}{RT}\right]$$
for $Zr_{0.89}Y_{0.08}Al_{0.03}O_{1.95}$ (10)

$$P_h^{1/4} = 1.09 \times 10^{-2}\, T \exp\left[\frac{10.2\,\text{kcal mol}^{-1}}{RT}\right]$$
for $Zr_{0.85}Ca_{0.15}O_{1.85}$ (11)

The oxygen permeation flux through $Zr_{0.85}Ca_{0.15}O_{1.85}$ ceramics at the constant oxygen pressure gradient of 0.21 atm/2.1×10^{-3} atm may be approximated in the temperature range 1000–1400 °C by [158]:

$$j_{o_2} d\,(\text{mol s}^{-1}\,\text{cm}^{-1}) = (20.2 \times 10^{-6})\, T \times \exp\left[-\frac{56.4 \pm 3.5\,\text{kcal mol}^{-1}}{RT}\right] \quad (12)$$

Samokhval et al. [158] showed also that the relationship between oxygen permeability and electron hole conductivity of oxygen solid electrolytes a constant quantity which is a function of temperature and material properties only.

Gilderman et al. [159] have studied oxygen permeation through the solid electrolyte $Zr_{0.85}Ca_{0.15}O_{1.85}$ caused by n-type electronic conductivity, at air/(H_2 + H_2O) gradients. The values of the specific oxygen partial pressure P_e (atm), at which the electronic conductivity is equal to the ionic conductivity, was found to be as follows:

$$P_e^{-1/4} = 4.2 \times 10^{-7}\, T \exp\left[\frac{60.8 \pm 3.6\ \text{kcal mol}^{-1}}{RT}\right] \quad (13)$$

Adding small amounts (0.1–0.2 wt%) of Bi_2O_3, Cr_2O_3, Fe_2O_3, or CuO did not result in significant changes of the oxygen permeability of $Zr_{0.90}Y_{0.10}O_{1.95}$ at 1000–1500 °C [160]. The doping with Mn_2O_3 and TiO_2 was observed to increase the permeability at temperatures below 1300 °C, whereas the effect of manganese oxide additions is much higher than that due to titania. Vanadium oxide additions lead to an increase in oxygen permeation fluxes at temperatures above 1400 °C.

Oxygen exchange between stabilized zirconia and gas phase

Exchange in atmosphere containing molecular oxygen

Studies by Kurumchin et al. [161–169] by the isotopic method showed that the oxygen exchange (OE) between zirconia-based solid electrolytes and a gas phase predominantly involves two oxygen ions of the oxide surface layer lattice. Contribution to the mechanism via interaction of one lattice ion with an adsorbed oxygen molecule increases with decreasing temperature and increasing oxygen partial pressure. The factor determining the OE rate was demonstrated to be electronic conductivity of the electrolyte surface [161, 162]. Thus, the OE rate of stabilized zirconia is much lower than that of CeO_2- and Bi_2O_3- based electrolytes (Fig. 3). There is a correlation between oxygen permeability caused by p-type electronic conduction and the exchange rate of the solid electrolytes (compare Figs. 2 and 3). In particular, oxygen permeation fluxes and the OE rate of ZrO_2-Sc_2O_3 ceramics are significantly lower than those of ZrO_2-CaO. For the zirconia electrolytes, surface locations active in the exchange reaction were found to be associated with stabilizing the cation sites [161].

Depositing electrode layers of electronic or mixed conductors (Pt, Ag, $La_{0.7}Sr_{0.3}CoO_{3-\delta}$, PrO_x) onto stabilized zirconia surfaces leads to a sharp increase of the exchange currents [161]. For the ceramics with Pt layers, a significant increase in the OE rate is observed at an increasing density of the layers up to approximately 2 mg cm^{-2}, and further deposition of platinum does not result in increasing exchange currents. In this case the reaction mechanism is dissociative adsorption of oxygen on the metal surface with subsequent diffusion of oxygen

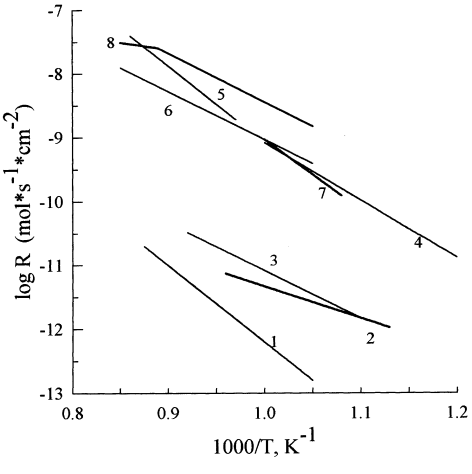

Fig. 3 Temperature dependence of the interphase oxygen exchange rate of solid electrolytes at an oxygen partial pressures of 1.3×10^{-2} atm [171, 172]: *1* $Zr_{0.906}Sc_{0.094}O_{1.953}$, *2* $Zr_{0.85}Ca_{0.15}O_{1.85}$, *3* $Zr_{0.90}$-$Y_{0.10}O_{1.95}$, *4* $Bi_{0.8}Er_{0.2}O_{1.5}$, *5* $Ce_{0.85}La_{0.15}O_{2-\delta}$, *6* $Zr_{0.90}Y_{0.10}O_{1.95}$ with an applied Pt layer (about 0.5 mg cm^{-2}), *7* $Bi_{0.8}Er_{0.2}O_{1.5}$ with an applied Pt layer, *8* $Zr_{0.906}Sc_{0.094}O_{1.953}$ with an applied Pt layer

atoms to the three-phase boundary [161, 164, 167]. For the silver layers, this mechanism is combined with dissolving oxygen in silver and diffusion through the silver layer. In the case of the $La_{0.7}Sr_{0.3}CoO_{3-\delta}$ perovskite layers deposited onto a YSZ surface, the exchange reaction was found to be localized at the cobaltite surface, and exchange properties of the electrode system coincide very closely with those of the lanthanum-strontium cobaltite specimens.

The exchange currents, calculated from the polarization resistance of platinum electrodes applied onto YSZ ceramics, were demonstrated to agree within experimental error limits with the OE rates of the same specimens measured by isotopic exchange [166, 168].

OE between stabilized zirconia and carbon oxides

OE rates of the stabilized zirconia electrolytes with CO_2 and CO are essentially higher than those with molecular oxygen [161, 170, 171]. This is especially pronounced for CO_2, which exchanges oxygen with YSZ 100 times faster than molecular oxygen under the same conditions. The interaction of zirconia with CO_2 and CO occurs via formation of carbonate complexes on the oxide surface and their subsequent decomposition. Studies by the isotopic carbon exchange method showed that the redox reaction in the CO_2-CO mixtures (the $CO_2 \Leftrightarrow CO$ conversion) on the YSZ surface is much slower than OE between zirconia and carbon oxides, i.e. the presence of one of the carbon oxides in the atmosphere does not affect the OE rate of another carbon oxide [170].

Analogously to molecular oxygen-containing atmosphere, a deposition of platinum or silver onto a stabilized zirconia surface was observed to lead to an increase of the OE rate between zirconia and carbon oxides [161, 179]. However, this effect is fairly weak in the case of CO_2-containing atmospheres. For instance, applying a platinum layer with a density of about 2 mg cm^{-2} resulted in an increase of the OE rate between O_2 and $Zr_{0.90}Y_{0.10}O_{1.95}$ at 1176 K by factor of approximately 3×10^2, between CO and $Zr_{0.90}Y_{0.10}O_{1.95}$ by a factor of 1×10^2, and between CO_2 and $Zr_{0.90}Y_{0.10}O_{1.95}$ by a factor of 3 [161]. The redox reaction rate in the CO-CO_2 mixtures also increases considerably after platinum layer deposition [170].

Electrodes in contact with stabilized zirconia

This part of the review is primarily devoted to metal and cermet electrodes in contact with stabilized zirconia ceramics. Properties of the perovskite electrodes will be considered in part II. A detailed analysis of the experimental and theoretical data of different electrode systems has been presented [1–3, 172].

Low-temperature limit of electrode reversibility

The technique proposed by Perfilyev et al. [173–175] to determine the reversibility of electrodes at lower temperatures is based on measuring the thermo EMF of the cells with two electrodes which are deposited onto electrolyte ceramic specimens and subjected to a temperature gradient in the same atmosphere. The temperature of the reference electrode (RE) is higher than that of the working electrode (WE) by ~150 °C in order to provide reversibility of the RE, while the WE may be irreversible. The cell should be gradually cooled, starting from high temperatures when both electrodes are reversible. The electrode potential at a given temperature can be represented as follows

$$\varphi = \varphi_{O_2} + \varphi_{ox} \tag{14}$$

where φ_{O_2} is the standard potential of oxygen electrode at the oxygen partial pressure of 1 atm, and φ_{ox} is its redox potential. The Seebeck coefficient of the cell (Θ) is given by the formula

$$\Theta = \Theta_{O_2} + \frac{d\varphi_{ox}}{dT} \tag{15}$$

where Θ_{O_2} is the Seebeck coefficient at the standard p_{O_2} value. Θ_{O_2} can be described by [1]

$$\Theta_{O_2} = A + \frac{R}{2F} \ln \frac{[V^{\bullet\bullet}]}{[O^{\times}]} + \frac{5R}{8F} \ln T + \frac{Q^*}{2FT} \tag{16}$$

where A is a constant independent of temperature, $[V^{\bullet\bullet}]$ is the mobile oxygen ion vacancy concentration, $[O^{\times}]$ is the oxygen ion concentration in the electrolyte, and Q^* is the heat of transport. If the oxygen ion vacancy concentration decreases with reducing temperature owing to the formation of defect associates, one can assume

$$[V^{\bullet\bullet}] = [V^{\bullet\bullet}]_0 \exp\left(-\frac{v}{RT}\right) \tag{17}$$

where $[V^{\bullet\bullet}]_0$ is the concentration of anion vacancies caused by stabilizing addition, and v is the dissociation energy for the defect associates. One can obtain the equation for an arbitrary atmosphere

$$\Theta = A + \frac{R}{2F} \ln \frac{[V^{\bullet\bullet}]_0}{[O^{\times}]} + \frac{5R}{8F} \ln T + \frac{Q^* - v}{2FT} + \frac{d\varphi_{ox}}{dT} \tag{18}$$

Here, v is equal to zero if the oxygen vacancy concentration is independent of temperature. The values of $d\varphi_{ox}/dT$ can be separately determined [176]. Integrating Eq. 18 with respect to temperature gives the expression for the theoretical thermo-EMF, E_T:

$$E_T = \left(a + \frac{d\varphi_{ox}}{dT}\right)(T_h - T_c) + b \ln \frac{T_h}{T_c} + \frac{5R}{8F}(T_h \ln T_h - T_c \ln T_c) \tag{19}$$

$$a = \frac{R}{T}\left(A + \frac{1}{2}\ln\frac{[V^{\bullet\bullet}]_0}{[O^{\times}]} - \frac{5}{8}\right) \quad (20)$$

$$b = \frac{Q^* - v}{2F} \quad (21)$$

where a and b are constants independent of temperature, and T_h and T_c are the temperatures of the RE and the WE, respectively. In order to analyze experimental values of the thermo-EMF E_{exp}, the following rearrangement is required:

$$y = -\frac{E_{exp}}{T_h - T_c} + \frac{5R}{8F} \times \frac{T_h \ln T_h - T_c \ln T_c}{T_h - T_c} + \frac{d\varphi_{ox}}{dT} \quad (22)$$

$$x = \frac{1000}{T_h - T_c}\ln\frac{T_h}{T_c} \quad (23)$$

In the case that the temperatures of both electrodes are sufficiently high and that there is equilibrium at both electrodes ($E_{exp} = E_T$), y is a linear function of x:

$$y = -\frac{b}{1000}x - a \quad (24)$$

In the course of the experiment [173], the working electrode state was considered to be irreversible if the deviation of the thermo-EMF of the cell from the linear model described by Eq. 24 is more than 1 mV. Typical temperature dependences of the thermo-EMF related to the y versus x coordinates are shown in Fig. 4.

Table 6 presents data on the low-temperature limit of reversibility of different metal electrodes as well as electrodes with mixed conductor additions. The measurements were performed using the solid electrolyte $Zr_{0.93}Y_{0.07}O_{1.925}$. Electrodes with a density of 20 mg cm^{-2} were made from a mixture of metal powders prepared by chemical precipitation and 15 wt% of the solid electrolyte powder. In the atmospheres containing free oxygen, praseodymia was used as the mixed conductor, and ceria was added to the electrode composition under a blanket of CO-CO_2 and H_2-H_2O.

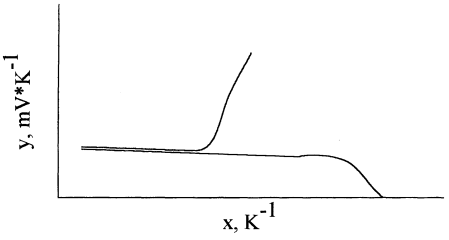

Fig. 4 Schematic drawing of the typical x-y dependences used to determine the low-temperature reversibility limit (see text)

For the platinum electrodes, the deviation of the electrode potential from the equilibrium value was explained by a slow attainment of electron hole equilibrium in the electrolyte [173]. For the silver and palladium electrodes, the factors determining the irreversibility were assumed to be decelerated equilibrium of oxygen dissolved in silver and a process of palladium oxidation, respectively. In the case of the addition of the mixed conductor, the OE between the mixed conductor and the gas phase is the process which determines electrode reversibility. The additions of praseodymia or ceria permit a considerable reduction of the low-temperature limit. A study of the behavior of an electrochemical sensor [177] confirmed the conclusions given [173] concerning the reversibility of porous platinum electrodes.

Electrode behavior of silver, palladium, and their alloys

Silver electrodes

Electrochemical properties of electrodes of silver and Ag-Pd alloys in contact with the ceramics $Zr_{0.91}Sc_{0.09}O_{1.955}$ and $Zr_{0.92}Y_{0.08}O_{1.96}$ and single crystals of $Zr_{0.90}Y_{0.10}O_{1.95}$ in atmospheres containing free oxygen were reported in research papers by Perfilyev and Lobovikova [178–183]. The specific behavior of the silver electrodes is determined by the high pressure of dissociation of silver oxide at 300–500 °C, by the high solubility of oxygen in metal silver at 400–900 °C, and by a decreasing melting point of the Ag-O_2 solid solutions with increasing oxygen content [178, 183]. As a

Table 6 Low-temperature limit of the electrode reversibility (°C) determined by the thermo-EMF method [173][a]

Electrode	Inert gas-O_2 (%O_2)					CO-CO_2 (%CO_2)					H_2-H_2O (%H_2O)					
	100	21	1	0.1	0.01	95	80	50	20	5	95	80	50	20	5	1
Pt	470	500	560	570	570	I	I	I	I	I	370	360	350	340	350	380
Au	530	510	I	I	I	610	610	600	600	590	470	380	320	310	350	410
Ag	510	530	600	670	730	I	I	I	I	I	380	360	340	360	350	300
Pd	590	600	620	620	600	I	I	I	I	I	490	470	470	500	510	490
Ni	n/a	n/a	n/a	n/a	n/a	570	590	610	650	690	n/a	n/a	n/a	n/a	n/a	n/a
Electrode with mixed conductor																
Pt	380	430	500	520	520	630	620	610	610	600	360	350	340	340	290	290
Au	390	420	480	540	600	520	500	490	480	480	480	430	400	370	330	280
Ag	350	430	570	600	590	520	520	550	600	660	400	380	370	360	300	n/a
Pd	360	460	570	570	490	670	650	630	600	530	340	360	380	370	330	n/a
Ni	n/a	n/a	n/a	n/a	n/a	660	660	640	600	590	n/a	n/a	n/a	n/a	n/a	n/a

[a] I indicates electrodes which are irreversible at temperatures below 800 °C. n/a means that the measurement was not performed

result, silver electrodes being polarized for a longer time were demonstrated to segregate into two layers, caused by the formation and decomposition of gaseous silver oxide [184]. The first layer, which is relatively thin and dense, is situated adjacent to the electrolyte surface, whereas the second layer exhibits high porosity, friability, and weak adhesion with the electrolyte. The thickness of the dense layer increases with the increasing temperature of the experiment. Along with this, no formation of the dense layers was observed in atmospheres with reduced oxygen partial pressures. The rate of evaporation of the silver electrode was found to decrease drastically within the first 400–600 h of polarization at 850 °C and then to stabilize at (3–5) $\times$ 10^{-6} g cm^{-2} h^{-1} [184].

The high solubility and diffusion mobility of oxygen in silver allow the assumption that oxygen diffusion through the silver layer is the limiting rate factor of the silver electrode [178, 183–185]. For the diffusion-limited kinetics of silver electrodes, the following equation was proposed to describe the dependence of the current on the overpotential [178, 179]:

$$I = \frac{SD_o}{A\delta} \times C_o\sqrt{p_{O_2}} \times \left(\exp\left[\frac{2F\eta}{RT}\right] - 1\right) \qquad (25)$$

where S is the electrode area, δ is the effective thickness of the diffusion layer, A is the electrochemical equivalent, D_o is the diffusion coefficient of oxygen in silver, and C_o is the solubility coefficient of oxygen in silver at a given temperature.

In a case of porous silver electrodes, limiting cathodic currents were observed, which indicated that oxygen diffusion is the limiting stage of the electrochemical process [178]. The dependences of $\ln(i_{lim}) = f(1/T)$, where i_{lim} is the limiting cathodic current, are linear and give an activation energy of 107 ± 8 kJ mol^{-1}. Although the slope of $\ln(i_{lim}) = f(\ln(p_{O_2}))$ is linear, and, as a rule, close to 1/2, Eq. 25 did not adequately describe the experimental tests [178]. There indicated that there is, along with the oxygen diffusion, another limiting stage for the cathode process. The cathodic polarization resistance of the porous silver layers was calculated to be in the range of 1–15 cm^{-2}. Additions of bismuth oxide to the silver electrodes were shown to reduce the cathodic polarization at temperatures below 750 °C [185]. An increasing temperature results in decreasing the effect of bismuth oxide owing to its evaporation.

Numerous studies of anodic polarization of porous silver electrodes demonstrated a melting of the silver, which was observed by optical microscopy *in situ* as well as after cooling of the electrochemical cell [178–180]. The polarization curves had a typical S-shape (Fig. 5), and could be characterized by the electrode potentials φ_1 and φ_2 which correspond to discontinuities of the current [178]. At potentials $\varphi < \varphi_1$, the limiting stage of the anode process is oxygen diffusion through silver. In the range $\varphi_1 < \varphi < \varphi_2$, oxidation of silver takes place in the near-electrolyte domain. This is accompanied by partial melting of the silver layers as well as exfoliating

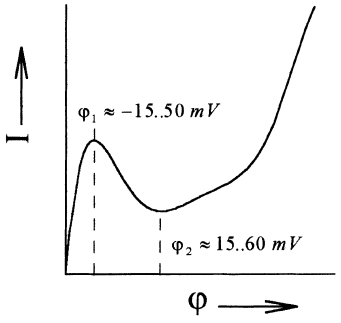

Fig. 5 Characteristic S-type polarization curves of silver electrodes (see text)

of the electrodes. A slow attainment of a steady and current pulsations may be observed. For electrode potentials higher than φ_2, improved contact between the electrode was explained to be a result of partial ionization of oxygen adsorbed at the silver surface [178].

Studies of silver migration at the electrode surface that Ag^+ ions are the mobile species present [185]. The formation of these ions is associated with intermediate formation of Ag_2O-like silver oxides. This explanation is confirmed by an absence of silver migration in a hydrogen atmosphere and in a vacuum [185].

Electrodes of Ag-Pd alloys

Owing to the oxidation of palladium, which leads to destruction of the electrode, palladium electrodes are of negligible interest for practical applications [2, 178]. Impedance spectroscopy of Pd electrodes deposited onto single crystals of $Zr_{0.90}Y_{0.10}O_{1.95}$ at 960 and 1100 °C in air has demonstrated that oxygen adsorption and diffusion at the electrode are the limiting stages of the electrode reaction [186].

Analogously to palladium metal, the Ag-Pd alloys are oxidized in oxygen-containing atmospheres at temperature below a specific temperature T_{ox} [178, 183]. Studies of the oxidation temperature using the cell

$$PdO,Ag\text{-}Pd,(Pt)|Zr_{0.91}Sc_{0.09}O_{1.96}|(Pt),air$$

showed a break of the composition dependence of T_{ox} at approximately 40 at% palladium. At temperatures above T_{ox} and in an oxidizing atmosphere, the polarization resistance (ρ_p) of the Ag-Pd electrodes is independent of time and the dependence $\ln(\rho_p) = f(1/T)$ is linear. Here, the electrode processes are limited by oxygen adsorption on palladium with subsequent diffusion to the three-phase boundary. At $T < T_{ox}$, oxidation of the electrodes accompanied by an increase of the polarization resistance by a factor of 10–100 with time was observed [178]. Cathodic polarization of the electrodes results in a reduction of the electrode material at potentials corresponding to the Pd/PdO electrode potential.

For silver-rich alloys, the dependences of the overpotential versus current density are close to those of

silver electrodes, but the extreme on the polarization curves at φ_1 is associated with the formation of PdO as a separate phase [178]. Then, the electrode properties are determined by the palladium-depleted alloy. The palladium oxide formation promotes an exfoliation of the electrodes. The stability of Ag-Pd electrodes can be improved by addition of solid electrolyte powder and praseodymia to the electrode composition [178].

Kinetics of the platinum electrode in oxygen-containing atmospheres.

At high oxygen pressures, platinum electrodes in contact with zirconia electrolytes exhibit, as a rule, Tafel-type dependences of overpotential on current density (see, for instance, [1, 2]). The oxygen partial pressure dependences on the exchange currents possess a temperature-dependent maximum which is associated with a decreasing electrochemical activity of oxygen at the oxidizing surface of platinum [187–190]. The authors of the first publications proposed an assumption concerning surface oxidation [191–196]. They detected that the properties of porous platinum electrodes show poor reproducibility and vary in the course of the experiment. This observation is in excellent agreement with the results of studying the interaction of oxygen with a platinum surface [197].

According to the data concerning the polarization of a platinum electrode and oxygen adsorption on platinum obtained by the coulometric titration method, that are two states of adsorbed oxygen which differ in bonding energy [187, 189, 190]. The first state, having weak bonds with the surface, refers to an absorbed layer, and can be described by Langmuir's adsorption isotherm. The second state with strong bonds may be understood as oxygen dissolved in the surface layer of platinum, or as a surface oxide. Calculations of surface coverage with an adsorbed layer obtained from electrochemical data give results close to those calculated from the coulometric titration provided that the surface coverage Θ is smaller than 0.1. An increasing coverage leads to complex relationships between the data obtained by different methods. For relatively low oxygen partial pressures, dependences of the polarization resistance of the platinum electrodes on p_{O_2} can be described [190]

$$R_\eta = R_{\eta 1} + R_{\eta 2} = K_1 p_{O_2}^{-0.5} + K_2 p_{O_2}^{-1} \qquad (26)$$

where the term ($R_{\eta 1}$, K_1) corresponds to a pure electrochemical process, the second term ($R_{\eta 2}$, K_2) characterizes the flux of molecular oxygen in the pores of the electrode, and K_1 and K_2 are constants. A decreasing oxygen pressure results in an increasing contribution of the second process, which becomes significant at $p_{O_2} < 10^{-7}$ atm. The activation energy for the electrochemical reaction was determined to be about 140–150 kJ mol^{-1} [189, 190]. Limiting stages of the electrode reaction are either the diffusion of oxygen at the platinum surface or OE at the reaction centers in the immediate vicinity of the three-phase boundary [190]. The OE between the gas phase and the zirconia electrolyte was assumed to occur via reaction centers at the (100) crystallographic plane of platinum.

In order to investigate the properties of platinum electrodes in detail, studies of model systems using electrodes in the form of plates [189], a foil [198, 199], and a net [188] were performed. Studies of a platinum foil cathode in contact with the solid electrolyte $Zr_{0.90}Y_{0.10}O_{1.95}$ allowed determination of the electron and the electron hole conductivities of the oxide as well as the position of the p-n transition as a function of the chemical potential of oxygen [198]. Using a foil cathode, it was also found that the presence of water vapour at constant oxygen pressure leads to a decreasing polarisation which can be explained by depolarizing effect of electron hole and proton conductivities of the electrolyte [199].

Impedance spectroscopy of the cell with two dense platinum plates sandwiching a thin layer of $Zr_{0.90}Y_{0.10}O_{1.95}$ powder demonstrated that the most adequate equivalent circuit for the platinum electrode comprises an impedance Z_W with a constant phase angle (CPA) and an active resistance R_η connected in parallel [189]. Z_W is caused by non-stationary process such as changes of the surface charge or variation of the electrolyte surface non- stoichiometry. The R_η values suggest that the electrochemical reaction zone is very narrow and does not exceed several tens of angstroms from the three-phase boundary [189].

Shkerin [188] studied electrochemical model systems with platinum net electrodes and single-crystal electrolytes by impedance spectroscopy. The electrode impedance spectra were found to consist of a characteristic low-frequency and a high-frequency range. The high- frequency component (Y_o) described by a CPA element is characteristic for the Faradaic process. The temperature-dependent low-frequency component is observed at frequencies below 150 Hz and refers to an inductive resistance (R_L). For the $Zr_{0.90}Y_{0.10}O_{1.95}$ and $Hf_{0.85}Y_{0.15}O_{1.925}$ single-crystal electrolytes, no effect of the crystallographic faces on the electrochemical processes was observed [188]. The dependence $Y_0 \sim p_{O_2}^{-1/4}$ indicates the formation of an electrolyte surface band owing to charge carrier injection by the electrode. Shkerin has proposed the mechanism of oxygen transport through the gas/electrolyte boundary to be as follows: applying an external electric field results in the injection of charge carriers into the solid electrolyte which provides for OE between the gas phase and the oxide. Here, the electrochemical process is localized predominantly near the three-phase boundary. An increasing electrical field was assumed to lead to an increasing activity of the electrolyte and an enlarged surface area of the electrolyte which takes part in the OE process. A further increase of the electrical field results in a decreasing conductivity of the system

owing to platinum oxidation, eventually leading to an irreversible degradation of the electrode.

Kuzin et al. [200, 201] described the behavior of the CPA element of porous platinum electrodes deposited onto single crystals of $Zr_{0.90}Y_{0.04}Sc_{0.06}O_{1.95}$ studied by impedance spectroscopy. The CPA element was suggested to be a result of a non-uniform current distribution at the electrode surface.

Electrode processes in fuel gas atmospheres

In general, the overpotential-current dependences of metal electrodes in reducing atmospheres follow the Tafel equation at both anodic and cathodic polarization. An exception is the electrolysis of water vapour, which exhibits a discontinuity in the polarization curves [202–204]. For nickel electrodes in contract with stabilized zirconia, the bonding potential was established to correspond to the potential of zero charge and, hence, to the minimum of the electrode capacity [202, 203]. As a general rule, the electrochemical activity of the electrodes in $H_2 + H_2O$ gas mixtures is considerably higher than in $CO + CO_2$ mixtures [205, 206]. The polarization resistance in $CO + CO_2$ mixtures is typically by a factor of 4–5 higher than in case of $H_2 + H_2O$. For nickel cermet electrodes, the activation energy for the anodic polarization resistance was calculated to be 155–160 kJ mol^{-1} in mixtures of $H_2 + H_2O$ and $H_2 + H_2O + CO + CO_2$, whereas it reached 190 kJ mol^{-1} in $CO + CO_2$ atmospheres [206]. The electrochemical activity of the electrodes increases regularly with increasing porosity [2, 207–211].

The dependence of the polarization resistance on the gas phase composition is complex and depends on the limiting stages of the electrode process, involving chemical reactions, diffusion, charge transfer, and adsorption [202, 205–207, 212, 213]. Thus, platinum electrodes exhibit minimum polarization resistance at concentrations of 50–60% of the reduced forms (CO, H_2) in the gas phase, whereas the polarization resistance of nickel cermet electrodes increases monotonically with increasing partial pressure of hydrogen or carbon monoxide [206, 214, 215]. For the $H_2 + H_2O + CO + CO_2$ mixtures with a high hydrogen content, the rate of the electrochemical process is determined by the reaction $O^{2-} + H_2 \rightarrow H_2O + 2e^-$ [206]. At constant potential the rate of anodic processes increases, as a rule, with increasing pressure of the oxidizable component [2, 207, 208, 212, 213].

Additions of a mixed conductor (cerium oxide) to metal electrodes permit a drastic reduction of the electrode polarization [205, 216]. Thus, the polarization resistance of cermet electrodes containing platinum and $Zr_{0.91}Sc_{0.09}O_{1.955}$ was shown to decrease by the incorporation of ceria by a factor of 3–4 in the atmospheres of 50% CO-50% CO_2 and by a factor of 4–5 in mixtures of 50% H_2 + 50% H_2O [205]. The application of the mixed conductor reduces the polarization caused by the chemical reactions, but may result in increasing the diffusion limitations.

Somov and Perfilyev [216] have studied the polarization characteristics of cathodes of Pi, Pd, Ni, Ag, and Cu with additions of zirconia solid electrolyte and ceria. Introducing the mixed-conducting oxide into electrodes was shown to result in a considerable decrease of the polarization resistance (by a factor of 10^3 for the copper electrodes). Such doping also leads to levelling of the polarization resistances of different metals. Thus, if the difference between the polarization resistance of different metals reaches 100 (nickel and copper), the maximum difference between the doped electrodes does not exceed 2. The polarization mechanism was also changed with the addition of ceria. The ceria-doped electrodes were shown to exhibit linear dependences of the overpotential on the current density within a wide current range, while the Tafel-type dependences are typical for the electrodes without additions [216]. As increasing ionic conductivity of the mixed conductor leads to a further decrease of the polarization, the limiting stage of the doped electrodes was assumed to be the oxygen transport through the mixed conductor to the electrolyte.

The electrochemical activity of both platinum and nickel electrodes is a function of their pre-history, which determines their oxidation state [202, 217]. As a rule, annealing electrodes in a reducing atmosphere results in decreasing polarization resistance, whereas the effect of oxidizing gas mixtures is the opposite. One can oxidize or reduce the electrode by anodic or cathodic currents, respectively [202, 218, 219]. An important role in electrode behavior is the formation of graphite as a product of the electrochemical reduction of carbon oxides [209, 214, 220, 221].

When reducing $CO + CO_2$, mixtures using solid-electrolyte cells, the overpotential of carbon reduction on platinum electrodes is higher than on palladium [222, 223]. This is caused by the relatively high solubility of carbon in palladium. At potentials close to equilibrium, the carbon reduction rate was demonstrated to be proportional to the overpotential.

Perfilyev [217] has proposed the use of fuel electrodes with enlarged surface areas, which comprise a porous underlayer of the high-conducting electrolytes ZrO_2-CaO, ZrO_2-Y_2O_3, ZrO_2-Yb_2O_3, or ZrO_2-Sc_2O_3 deposited and sintered onto the surface of the ceramics of $Zr_{0.90}Y_{0.10}O_{1.95}$. Mixtures of metals (Pt, Pd, Ag, Ni, Cu) and electrolyte powder of the same composition as used to form the underlayer were deposited onto the surface of the underlayer. The polarization resistance was found to be independent of the electrolyte composition within the limits of reproducibility. The activation energy of the polarization resistance at temperature above 800 °C decreases in the sequence Cu > Pd > Ag > Ni > Pt.

Interestingly, the electrochemical activity of cobalt-containing electrodes is essentially higher than that of nickel electrodes [117]. Both cobalt and nickel cermet anodes exhibit sufficient stability, being tested at 900–1300 °C in a hydrogen atmosphere in experiments lasting

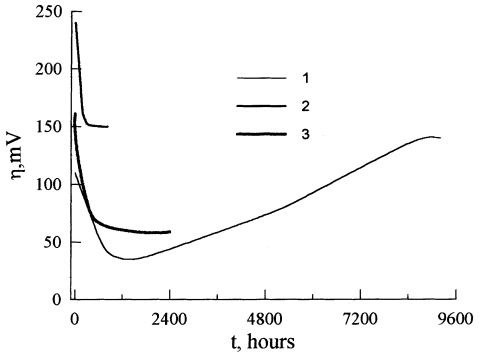

Fig. 6 Overpotential of different of SOFC deposited onto $Zr_{0.90}Y_{0.10}O_{1.95}$ electrolyte in flowing hydrogen at 1000 °C and at a current density of 100 mA cm^{-2} as a function of time, according to the data of Zhuravlev et al. [117]: *1* cobalt anode at 1000 °C, *2* nickel anode at 1000 °C, *3* nickel anode at 1100 °C

for 10 000 h. Decreasing polarization of the electrodes with time (Fig.6) was found to be caused by growing of the pore size from 2–5 to 5–10μm.

Oxidative conversion of methane in SOFC with zirconia electrolyte

Studies of methane oxidation on metal electrode catalysts of Ag, Au and Ag-1 wt% Ni deposited onto $Zr_{0.90}Y_{0.10}O_{1.95}$ electrolyte demonstrated the potential ability of simultaneous methane conversion and power generation using SOFC-type reactors [224–230]. The C_2 hydrocarbon formation selectivity may be as high as 90% . For silver and gold electrodes under conditions where oxygen is transported into the reaction zone only through the electrolyte, an increasing current was shown to lead to an increasing oxidation rate and decreasing selectivity of the oxidative dimerization. In contrast, maximum dimerization selectivity can be achieved on the nickel-containing electrodes with periodical interruptions of the circuit [224]. The interruptions allow reduction of the nickel oxides which have been formed under anodic polarization. The higher rate and selectivity of the formation of C_2 hydrocarbons by the electrocatalytic methane oxidation in comparison to the catalytic oxidation were shown to be due to the existence of active oxygen species at the electrode surface.

An additional oxygen supply through the solid electrolyte into the mixture of oxygen and methane did not result in a considerable change of the methane oxidation rate [224, 227–229]. At the same time, pumping of the oxygen from the mixture leads to a sharp increase of the conversion rate, exhibiting the effect of non-Faradaic electrochemical modification of catalytic (NEMCA). This effect was most pronounced for the oxidation of carbon monoxide [229].

By the oxygen isotopic exchange method it was shown that the bond strength of oxygen adsorbed on the platinum electrode is not changed when current is flowing through the cell [230]. This indicates that the changing catalytic properties with respect to the oxidation reactions are not a direct consequence of the polarization [224, 230]. The idea that the electrochemical reduction of oxygen at metal electrodes initiates chain oxidation reactions of methane and CO was proposed to explain the NEMCA effect [224].

Reference

1. Chebotin MV, Perfilyev MV (1978) Electrochemistry of solid electrolytes (in Russian). Khimiya, Moscow
2. Perfiliev MV, Demin AK, Kuzin BL, Lipilin AS (1988) High-temperature electrolysis of gases (in Russian). Nauka, Moscow
3. Murygin IV (1991) Electrode processes in solid electrolytes (in Russian). Nauka, Moscow
4. Toropov NA, Barzakovskii VP, Lapin VV, Kurtseva NN (1969) Phase diagrams of silicate systems. A handbook, vol 1. (in Russian). Nauka, Leningrad
5. Kravchinskaya MV (1985) Zirconate systems In: Galakhov FYa (ed) Phase diagrams of high-melting oxide systems. A handbook, vol 5 (in Russian). Nauka, Leningrad, pp 303–338
6. Popova LN (1970) PhD Thesis, Moscow State University, Moscow
7. Palguev SF, Gorelov VP, Volchenkova ZS (1973) Tr Inst Elektrokhim Ural Akad Nauk SSSR 20: 140–144
8. Volchenkova ZS (1973) Tr Inst Elektrokhim Ural Akad Nauk SSSR 19: 100–105
9. Volchenkova ZS (1974) Tr Inst Elektrokhim Ural Akad Nauk SSSR 21: 108–117
10. Vakulenko AM (1995) PhD Thesis, Russian Academy of Sciences, Moscow
11. Volchenkova ZS, Nedopekin VM (1974) Neorg Mater 10: 1821
12. Gorelov VP (1980) PhD Thesis, Ural Dept. of the Academy of Sciences of USSR, Sverldovsk
13. Gorelov VP (1978) Tr Inst Elektrokhim Ural Akad Nauk SSSR 26: 69–75
14. Ezersky ML, Kozlova II, Popilsky RYa, Demonis IM (1968) Neorg Mater 4: 1599
15. Nikolsky YuV, Filatov SK, Zhuravina TA, Frank-Kamenetsky VA (1972) Neorg Mater 8: 1500
16. Kuznetsov AK, Zimina LA, Keler EK (1968) Neorg Mater 4: 1112
17. Lukin ES, Borovkova AB, Khudak EB (1974) Neorg Mater 10: 1911
18. Neuimin AD, Palguev SF (1964) Tr Inst Elektrokhim Ural Akad Nauk SSSR 5: 145–151
19. Volchenkova ZS (1969) Tr Inst Elektrokhim Ural Akad Nauk SSSR 12: 114–119
20. Volchenkova ZS (1968) Neorg Mater 4: 1975
21. Leonov AI, Andreeva AB, Keler EK (1966) Neorg Mater 2: 137
22. Filatov SK, Frank-Kamenetsky VA, Zhuravina TA (1969) Krist Techn 2: S.311
23. Klucharov YaV, Strakhov VI (1970) Ogneupory No 1: 40
24. Keler EK, Andreeva AB (1963) Ogneupory No 5: 224
25. Krasilnikov MD (1978) PhD Thesis, Academy of Sciences of USSR, Leningrad
26. Strekalovsky VN, Volchenkova ZS, Samarina VA (1965) Neorg Mater 1: 1372
27. Volchenkova ZS (1966) Tr Inst Elektrokhim Ural Akad Nauk SSSR 9: 139–148
28. Vinokurov IV, Krasilnikov MD, Altukhov VG, Tikhonov PA (1976) In: Construction and technical materials from non-metalliferous mineral resources (in Russian). Nauka, Moscow, pp 76–85

29. Volchenkova ZS (1967) In: Chemistry of high-temperature materials (in Russian). Nauka, Leningrad, pp 65–69
30. Davtyan IA, Glushkova VB, Keler EK (1965) Neorg Mater 1: 743
31. Glushkova VB, Davtyan IA, Keler EK (1965) Neorg Mater 1: 1955
32. Sazonova LV, Davtyan IA, Glushkova VB (1965) Neorg Mater 1: 1965
33. Scherbakova LG, Lobachev AN, Kuznetsov VA (1975) Dokl Akad Nauk SSSR 225: 890
34. Zoz EI, Fomichev EN, Kalashnik AA (1982) Zh Heorg Khim 27: 1995
35. Volchenkova ZS (1970) Tr Inst Elektrokhim Ural Akad Nauk SSSR 14: 125–128
36. Volchenkova ZS (1972) Tr Inst Elektrokhim Ural Akad Nauk SSSR 18: 138–143
37. Dmitriev VI, Surkov ME, Kostukov MS, Kharitonov FYa, Maslennikova GN, Shashkova VI (1973) Elekron Tekhm Ser Mater 12: 99
38. Surkov ME, Kharitonov FYa, Esikov YuG, Maslennikova GN (1973) Elektron Tekh Ser Mater 10: 94
39. Kiparisov SS, Belyaev RA, Belyakov AI, Bondarenko VV, Vyskubov VI, Kozlov VG, Kuznetsov SA, Melikhova LI (1976) Neorg Mater 12: 1693
40. Gorelov VP, Palguev SF (1979) Dokl Akad Nauk SSSR 248: 1356
41. Strekalovsky VN, Polezhaev YuM, Palguev SF (1987) Oxides with impurity-caused disorder. Composition, structure, phase transitions (in Russian). Nauka, Moscow
42. Palguev SF, Fomina LN, Strekalovsky VN (1973) Tr Inst Elektrokhim Ural Akad Nauk SSSR 19: 120–127
43. Fomina LN (1973) PhD Thesis, Ural Dept. of the Academy of Sciences of USSR, Sverdlovsk
44. Ioffe AI, Rutman DS, Karpachov SV (1978) Electrochim Acta 23: 141
45. Ioffe AI (1977) PhD Thesis, Moscow State University, Moscow
46. Lipilin AS, Neuimin AD, Palguev SF (1976) Tr Inst Elektrokhim Ural Akad Nauk SSSR 24: 72–77
47. Vakulenko AM, Lobkovsky EB, Torbova OD, Berestenko VI (1989) Elektrokhimiya 25: 680
48. Alekseenko LS, Gudilina AI, Tyagileva LV (1976) In: Production of special refractories, vol 3 (in Russian). Metallurgiya, Moscow, pp 5–10
49. Aleekseenko LS, Koifman GYu, Posokhova ED, Shakhtin DM (1974) Neorg Mater 10: 2006
50. Lidorenko NS, Kagan AS, Bykovskaya LA, Efimovskaya TV, Lutsareva LA, Chizhik SP, Shumanova SP (1969) Dokl Akad Nauk SSSR 187: 791
51. Ovchinnikov YuM, Neuimin AD, Palguev SF, Lipilin AS (1969) Elektrokhimiya 5: 1224
52. Vlasov AN (1989) Elektrokhimiya 25: 1313
53. Vlasov AN (1989) Elektrokhimiya 25: 699
54. Volchenkova ZS, Nedopekin VM, Gorelov VP, Palguev SF (1978) Neorg Mater 11: 1424
55. Chebotin VN (1982) Physical chemistry of solid state (in Russian). Khimiya Moscow
56. Inozemtsev MV, Lipilin AS, Perfilyev MV (1976) Tr Inst Elektrohim Ural Akad Nauk SSSR 23: 117–121
57. Inozemtsev MV, Perfilyev MV, Lipilin AS (1976) Tr Inst Elektrokhim Ural Akad Nauk SSSR 23: 122–125
58. Redko VP (1990) PhD Thesis, Ukrainian Academy of Science, Kiev
59. Zyrin AV, Redko VP, Lopato LM (1987) Neorg Mater 23: 1325
60. Redko VP, Lopato LM (1990) Dokl Akad Nauk USSR Ser A No 4: 78
61. Lopato LM, Redko VP, Gerasimyuk GI, Shevchenko AV (1990) Poroshk Metall No 4: 73
62. Neuimin AD, Lipilin AS, Palguev SF, Gulbis FYa (1975) In: Melted and solid electrolytes (in Russian). Academy of Sciences of USSR, Ural Dept., Sverdlovsk pp 123–134
63. Perfilyev MV, Inozemstev MV, Alekseenko LS, Evlampiev AI, Fadeev GI (1979) In: Melted and solid electrolytes (in Russian). Academy of Sciences of USSR, Ural Dept., Sverdlovsk, pp 96–106
64. Volchenkova ZS, Palguev SF (1961) Tr Inst Elektrokhim Ural Akad Nauk SSSR 2: 173–183
65. Keler EK, Godina NA (1955) Ogneupory No 9: 416
66. Gavrish AM, Sukharevsky BYa, Zoz EI, Krivoruchko PP (1969) Neorg Mater 5: 1584
67. Strekalovsky VN, Palguev SF (1970) In: X-ray difractometry of mineral resources, vol 7 (in Russian). Nedra Moscow, pp 30–46
68. Sukharevsky BYa, Gavrish AM, Zoz EI (1975) Neorg Mater 11: 465
69. Palguev SF, Neuimin AD, Strekalovsky VN (1966) Tr Inst Elektrokhim Ural Akad Nauk SSSR 9: 149–157
70. Gavrish AM, Zoz EI (1978) Neorg Mater 14: 181
71. Zoz EI, Lopato LM (1983) Neorg Mater 19: 1702
72. Godina NA, Keler EK (1961) Ogneupory No 9: 426
73. Sukharevsky BYa, Vishnevsky II, Gavrish AM (1961) Dokl Akad Nauk SSSR 140: 884
74. Levitsky VA, Khekimov Yu, Narchuk PB, Gerasimov YaI (1977) Zh Fiz Khim 51: 2553
75. Kachalova AP, Avgustinnik AI (1959) Zh Priklad Khim 32: 1451
76. Demonis IM, Popilsky RYa (1967) Tr Moskov Khim Tekhnol Inst 55: 151–156
77. Vlasov AN, Shulik IG (1988) Neorg Mater 24: 1849
78. Filatov SK, Frank-Kamenetsky VA (1969) Kristallografiya 14: 505
79. Filatov SK, Frank-Kamenetsky VA (1970) Kristallografiya 15: 176
80. Ezersky ML, Kozlova NI, Bagotsky VS, Kalliga GP, Demonis IM, Rastorguev LN, Prilepsky VI (1966) Neorg Mater 2: 1811
81. Kabanova IM (1990) PhD Thesis, Ukrainian Academy of Science, Kiev
82. Karaulov AG, Rudyak IN (1975) Ogneupory No 2: 54
83. Glumov MV, Neuimin AD, Palguev SF, Strekalovsky VN (1969) Tr Inst Elektrokhim Ural Akad Nauk SSSR 12: 130–134
84. Lipilin AS, Neuimin AD, Gulbis FYa (1975) In: Melted and solid electrolytes (in Russian). Academy of Sciences of USSR, Ural Dept., Sverdlovsky, pp 135–1377
85. Strekalovsky VN, Palguev SF, Zubankov VN (1970) Tr Inst Elektrokhim Ural Akad Nauk SSSR 14: 129–138
86. Krzhizhanovskaya VA, Glushkova VB, Keler EK, Scherbakova LG (1975) Neorg Mater 11: 471
87. Zubankov VN, Strekalovsky VN, Palguev SF (1969) Tr Inst Elektrokhim Ural Akad Nauk SSSR 13: 112–119
88. Zubankov VI, Strekalovsky VN, Palguev SF (1969) Neorg Mater 5: 88
89. Karaulov AG, Rudyak II, Taranukha IM, Glushko LI (1974) Neorg Mater 10: 1281
90. Fomina LN, Palguev SF, Strekalovsky VN, Lipilin AS, Rozanov IG (1973) Tr Inst Elektrokhim Ural Akad Nauk SSSR 20: 134–139
91. Zhidovinova SV (1974) PhD thesis, Ural Dept. of the Academy of Sciences of USSR, Sverdlovsk
92. Keler EK, Godina NA (1955) Dokl Akad Nauk SSSR 103: 247
93. Rutman DS, Toropov YuS, Polezhaev YuM (1981) In: Scientific basis of materials science (in Russian). Nauka, Moscow, pp 27–38
94. Ioffe AI, Strekalovsky VN, Rutman DS, Karpachev SV (1973) Dokl Akad Nauk SSSR 209: 646
95. Alekseenko LS (1967) PhD Thesis, Ukrainian Research Institute of Refractories, Kharkov
96. Alekseenko LS, Kaynarsky IS, Degtyareva EV (1996) Ogneupory No 12: 40
97. Kaynarsky IS, Alekseenko LS, Degtyareva EV (1967) Poroshk Metall No 4: 24
98. Kaynarsky IS, Alekseenko LS, Degtyareva EV (1967) Poroshk Metall No 7: 39

99. Inozemtsev MV, Perfilyev MV (1976) Elektrokhimiya 12: 1236
100. Ioffe AI, Inozemtsev MV, Lipilin AS, Perfilyev MV, Karpachov SV (1975) Phys Status Solidi A 30: 87
101. Perfilyev MV, Inozemtsev MV (1976) Tr Inst Elektrokhim Ural Akad Nauk SSSR 24: 95–110
102. Inozemtsev MV, Perfilyev MV, Gorelov VP (1974) Elektrokhimiya 10: 1471
103. Inozemtsev MV, Perfilyev MV (1975) Elektrokhimiya 11: 1031
104. Palguev SF (1978) Tr Inst Khim Ural Akad Nauk SSSR 36: 127–133
105. Karavaev YuN, Neuimin Ad, Palguev SF (1976) In: Studies of salt meltings and oxide systems (in Russian).Academy of Sciences of USSR, Ural Dept. Sverdlovsk, pp 103–108
106. Grebenyuk AA, Karaulov AG, Sudarkina TE (1974) In: Production of special refractories, vol 3 (in Russian). Metallurgiya, Moscow, pp 50– 66
107. Kotlyar AG, Neuimin AD, Palguev SF, Strekalovsky VN (1970) Neorg Mater 6: 532
108. Kotlyar AG (1969) PhD Thesis, Ural Dept. of the Academy of Sciences of USSR, Sverdlovsk
109. Sazonova LV, Glushkova VB, Keler EK (1976) Neorg Mater 12: 450
110. Kotlyar AG, Neuimin AD, Palguev SF, Strekalovsky VN, Zubankov VN (1970) Neorg Mater 6: 327
111. Perfilyev MV, Inozemtsev MV, Vlasov AN (1982) Elektrokhimiya 18: 1230
112. Vlasov AN, Inozemtsev MV (1985) Elektrokhimiya 21: 764
113. Vlasov AN (1983) Elektrokhimiya 19: 1624
114. Vlasov AN, Perfilyev MV (1989) In: Ionic meltings and solid electrolytes, vol 4 (in Russian). Navukova Dumka, Kiev, pp 55–63
115. Inozemtsev MV, Perfilyev MV, Gorelov VP (1976) Elektrokhimiya 12: 1231
116. Vlasov AN, Inozemtsev MV, Perfilyev MV (1985) Elektrokhimiya 21: 798
117. Zhuravlev BV, Gaag VA, Neuimin AD, Palguev SF (1981) In; Electrode processes in halide and oxide electrolytes (in Russian). Academy of Sciences of USSR, Ural Dept., Sverdlovsk, pp 97–103
118. Solov'eva LM (1970) PhD Thesis, Ural Dept. of the Academy of Sciences of USSR, Sverdlovsk
119. Shulik IG, Usatikov IF, Alekseenko LS, Orekhova GP, Kvasman NM, Kamenetsky YuL, Degtyareva EV (1987) Ogneupory No 10: 13
120. Kuznetsov AK, Krasilnikov MD, Tikhonov PA (1972) Neorg Mater 8: 79
121. Kotlyar AG, Neuimin AG, Palguev SF, Strekalovsky VN (1972) Tr Inst Elektrokhim Ural Akad Nauk SSSR 18: 144–147
122. Andrievskaya ER (1989) PhD Thesis, Ukrainian Academy of Science, Kiev, Ukraine
123. Lopato LM, Andrievskaya ER, Shevchenko AV (1988) Neorg Mater 24: 1861
124. Tikhonov PA, Kuznetsov AK, Keler EK (1971) Neorg Mater 7: 2015
125. Afanasyev SK, Saldau PYa (1950) Zap Leningrad Gorn Inst No 24: 139
126. Gavrish AM, Sukharevsky BYa, Zoz EI, Krivoruchko PP (1969) Neorg Mater 5: 1103
127. Berezhnoi AS, Kordyuk RA (1963) Dopo Akad Nauk URSR No 10: 1344
128. Berezhnoi AS, Tarnopolskaya RA (1968) Neorg Mater Akad Nauk 4: 2151
129. Tarnopolskaya RA, Gulko NV, Gavrish AM (1968) Dokl Akad Nauk SSSR 180: 1176
130. Berezhnoi AS, Kordyuk TA (1964) Dopo Akad Nauk URSR No 5: 506
131. Tarnopolskaya RA, Gulko NV (1966) Dokl Akad Nauk SSSR 170: 1380
132. Melnik MT, Ved EI, Ilyukha NG (1973) Neorg Mater 9: 332
133. Melnik MT, Ilyukha NG, Bershtein VL (1992) Ogneupory No 8: 54
134. Strakhov VI, Klyucharov YaV, Sergeev GG (1972) Neorg Mater 8: 578
135. Gavrish AM, Sukharevsky BYa, Zoz EI (1975) Dokl Akad Nauk SSSR 222: 1343
136. Gavrish AM, Sukharevsky BYa, Zoz EI, Solov'ea AE (1973) Neorg Mater 9: 2609
137. Toropov YuS, Pliner SYu, Rutman DS, Taksis GA, Maurin AF (1969) Ogneupory No 11: 49
138. Shvaiko-Shavikovsky VE, Keler EK, Leonov AI, Popov VI (1975) Dokl Akad Nauk SSSR 222: 1350
139. Filatova VN, Chernyshov GP, Valyano GE, Pankratyeva SV, Rautbort AE, Lukin BV, Rekov AI, Akopov FA (1975) Neorg Mater 11: 1427
140. Karavaev YuN, Neuimin AD, Palguev SF (1976) Tr Inst Elektrokhim Ural Akad Nauk SSSR 24: 86–94
141. Karavaev YuN, Neuimin AD, Palguev SF, Lakeeva ZN (1976) In: Studies of salt meltings and oxide systems (in Russian). Academy of Sciences of USSR, Ural Dept. Sverdlovsk, pp 95–102
142. Karavaev YuN, Neuimin AD, Palguev SF (1976) In: Studies of salt meltings and oxide systems (in Russian). Academy of Sciences of USSR, Ural Dept., Sverdlovsk, pp 109–116
143. Neuimin AD, Kotlyar AG, Palguev SF, Strekalovsky VN, Batrakov NA (1969) Tr Inst Elektrokhim Ural Akad Nauk SSSR 12: 93–113
144. Kotlyar AG, Neuimin AD, Palguev SF, Strekalovsky VN, Lakeeva ZN, Rozhdenstvensky FA (1970) Tr Inst Elektrokhim Ural Akad Nauk SSSR 16: 128–137
145. Neuimin AD, Karavaev YuN, Palguev SF (1974) Tr Inst Elektrokhim Ural Akad Nauk SSSR 21: 132–141
146. Neuimin AD, Palguev SF, Strekalovsky VN, Burov GV (1963) Tr Inst Elektrokhim Ural Akad Nauk SSSR 4: 83–90
147. Neuimin AD, Gilderman VK, Palguev SF (1974) Tr Inst Elektrokhim Ural Akad Nauk SSSR 21: 126–131
148. Smachnaya VF, Saldau PYa (1950) Zap Leningrad Gorn Inst No 24: 153
149. Gorelov VP (1988) Elektrokhimiya 24: 1380
150. Vecher DV (1970) PhD Thesis, Moscow State University, Moscow
151. Vecher AA, Vecher DV (1967) Zh Fiz Khim 41: 1288
152. Vecher AA, Vecher DV (1967) Dokl Akad Nauk BSSR 11: 610
153. Vecher AA, Vecher DV (1968) Zh Fi Khim 42: 799
154. Savitsky AA, Samokhval VV, Vecher AA (1976) Vestn Belorus Univ Ser 2 No 3: 3
155. Gilderman VK, Neuimin AD, Palguev SF (1974) Tr Inst Elektrokhim Ural Akad Nauk SSSR 21: 118–125
156. Ovchinnikov YuM, Karpachev SV, Neuimin AD, Palguev SF (1965) Ogneupory No 10: 40
157. Gilderman VK, Neuimin AD, Palguev SF (1974) Dok Akad Nauk SSSR 218: 133
158. Samokhval VV, Loiko GI, Vecher AA (1973) Zh Fiz Khim 47: 2275
159. Gildermann VK, Gilmizyanov L, Neuimin AD, Palguev SF (1979) Elektrokhimiya 15: 1206
160. Gilderman VK, Neuimin AD, Palguev SF, Toropov YuS (1976) Elektrokhimiya 12: 1585
161. Kurumchin EKh (1997) DSc Thesis, Institute of High-Temperature Electrochemistry RAS, Ekaterinburg
162. Kurumchin EKh (1990) In: Perfilyev MV (ed) Electrode reactions in solid electrolytes (in Russian). Academy of Sciences of USSR, Ural Dept., Sverdlovsk, pp 63–79
163. Kurumchin EKh, Perfilyev MV, Karpachev SV, Muzykantov VS (1976) Kine Katal 17: 1519
164. Karpachev SV, Kurumchin EKh, Perfilyev MV (1979) Kinet Katal 20: 123
165. Kurumchin EKh, Ischuk VP (1982) Kinet Katal 23: 1005
166. Gorelov VP, Kurumchin EKh, (1990) Elektrokhimiya 26: 1502
167. Gorelov VP, Kurumchin EKh, Vdovin GK (1992) Elektrokhimiya 28: 1476
168. Gorelov VP, Kurumchin EKh, Perfilyev MV (1992) Elektrokhimiya 28: 1576

169. Vdovin GK, Kurumchin EKh, Perfilyev MV (1993) Elektrokhimiya 29: 1366
170. Ischuk VP (1984) PhD Thesis, Ural State University, Sverdlovsk
171. Ischuk VP, Kurumchin EKh, Perfilyev MV, Karpachev SV (1980) Kinet Katal 21: 714
172. Palguev SF, Gilderman VK, Zemtsov VI (1990) High-temperature electronic conductors for electrochemical devices (in Russian). Nauka, Moscow
173. Fadeev GI, Perfilyev MV (1988) In: Perfilyev MV (ed) Electrode processes in solid-electrolyte systems (in Russian). Academy of Sciences of USSR, Ural Dept., Sverdlovsk, pp 85–95
174. Perfilyev MV, Fadeev GI (1990) Elektrokhimiya 26: 1322
175. Perfilyev MV, Fadeev GI (1977) In: Electrochemistry of high-temperature electrolytes (in Russian). Academy of Sciences of USSR, Ural Dept., Sverdlovsk, pp 102–106
176. Möbius H.-H. (1965) Z Phys Chem 230: 398
177. Kuzin BL, Komarov MA (1991) Elektrokhimiya 27: 1128
178. Lobovikova NA, Perfilyev MV (1988) In: Perfilyev MV (ed) Electrode processes in solid-electrolyte systems (in Russian). Academy of Sciences of USSR, Ural Dept., Sverdlovsk, pp 67–84
179. Perfilyev MV, Lobovikova NA (1975) In: Tr Inst Elektrokhim Ural Akad Nauk SSSR 22: 138–145
180. Perfilyev MV, Lobovikova NA (1984) Elektrokhimiya 20: 322
181. Lobovikova NA, Perfilyev MV (1981) In: Baraboshkin AN (ed) Electrode processes in halide and oxide electrolytes (in Russian). Academy of Sciences of USSR, Ural Dept., Sverdlovsk, pp 91–96
182. Lobovikova NA, Perfilyev MV (1993) In: Pefilyev MV (ed) Ionics of solid state (in Russian). Nauka, Sverdlovsk, pp 70–75
183. Lobovikova NA (1985) PhD Thesis, Academy of Sciences of USSR, Ural Dept., Sverdlovsk
184. Arzhannikov VA, Fedin VV, Neuimin AD, Palguev SF (1973) In: Physical chemistry of meltings and solid electrolytes (in Russian). Academy of Sciences of USSR, Ural Dept., Sverdlovsk, pp 88–94
185. Arzhannikov VA (1985) PhD Thesis, Academy of Sciences of USSR, Ural, Dept., Sverdlovsk
186. Antonov VA, Arsenyev PA, Bagdasarov KhS, Gruzdev AN, Malov MM, Ryazantsev AD (1981) Elektrokhimiya 27: 884
187. Kuzin BL, Komarov MA (1988) Elektrokhimiya 24: 201
188. Shkerin SN (1989) PhD Thesis, Academy of Sciences of USSR, Ural Dept., Sverdlovsk
189. Kuzin BL, Komarova NYu (1990) In: Perfilyev MV (ed) Electrode reactions in solid electrolytes (in Russian). Academy of Sciences of USSR, Ural Dept., Sverdlovsk, pp 25–36
190. Kuzin BL, Komarov MA (1991) In: Perfilyev MV (ed) Electrode processes of solid-state systems (in Russian). Academy of Sciences of USSR, Ural Dept., Sverdlovsk, pp 3–17
191. Filyaev AT, Karpachev SV, Palguev SF (1965) Tr Inst Elektrokhim Ural Akad Nauk SSSR 7: 169–174
192. Perfilyev MV, Palguev SF (1965) Tr Inst Elektrokhim Ural Akad Nauk SSSR 7: 157–162
193. Perfilyev MV, Palguev SF (1965) Tr Inst Elektrokhim Ural Akad Nauk SSSR 6: 107–114
194. Perfilyev MV, Palguev SF (1965) Tr Inst Elektrokhim Ural Akad Nauk SSSR 6: 115–121
195. Perfilyev MV, Palguev SF (1965) Tr Inst Elektrokhim Ural Akad Nauk SSSR 7: 163–168
196. Perfilyev MV, Palguev SF (1970) Tr Inst Elektrokhim Ural Akad Nauk SSSR 15: 141–143
197. Popova NM, Babenkova LV, Savelyeva GA (1979) Adsorption and interaction of simplest gases with VIII group metals (in Russian). Nauka, Alma-Ata
198. Glumov MV (1988) In: Perfilyev (ed) Electrode reactions in solid- electrolyte systems (in Russian). Academy of Sciences of USSR, Ural Dept., Sverdlovsk pp 46–57
199. Glumov MV, Brainin MI (1990) In: Perfilyev MV (ed) Electrode reactions in solid electrolytes (in Russian). Academy of Sciences of USSR, Ural Dept., Sverdlovsk, pp 50–57
200. Bronin DI, Kuzin BL (1992) Elektrokhimiya 28: 1499
201. Kuzin BL, Bronin DI (1997) Elektrohimiya 33: 572
202. Kuzin BL, Glumov MV (1976) Tr Inst Elektrokhim Ural Akad Nauk SSSR 24: 115–119
203. Kuzin BL, Glumov (1976) Tr Inst Elektrokhim Ural Akad Nauk SSSR 24: 120–124
204. Kuzin BL (1979) In: Proceeding of the VII conf. physical chemistry and electrochemistry of melted and solid electrolytes (in Russian). Academy of Sciences of USSR, Ural Dept., Sverdlovsk, pp 110–112
205. Perfilyev MV (1993) In: Perfilyev MV (ed) Ionics of solid state (in Russian). Nauka, Ekaterinburg pp 76–80
206. Kuzin BL, Beresnev SM (1997) Elektrokhimiya 33: 1480
207. Kuzin BL (1977) PhD Thesis, Academy of Sciences of USSR, Ural Dept., Sverdlovsk
208. Kuzin BL, Neuimin AD, Palguev SF (1973) Elektrokhimiya 9: 17
209. Zupnik AE (1971) PhD Thesis, Academy of Sciences of USSR, Ural Dept. Sverdlovsk
210. Chebotin VN, Glumov MV, Neuimin AD, Palguev SF (1971) Elektrokhimiya 7: 62
211. Zupnik AE, Perfilyev MV, Karpachev SV (1971) Elektrokhimiya 7: 1163
212. Filyaev AT, Palguev SF, Karpachev SV (1961) Tr Inst Elektrokhim Ural Akad Nauk SSSR 2: 199–209
213. Karpachev SV, Filyaev AT, Palguev SF (1962) Tr Inst Elektrokhim Ural Akad Nauk SSSR 3: 161–164
214. Kuzin BL, Bronin DI (1993) Elektrokhimiya 29: 279
215. Chebotin VN, Glumov MV, Palguev SF, Neuimin AD (1971) Elektrokhimiya 7: 196
216. Somov SI, Perfilyev MV (1990) In: Perfilyev MV (ed) Electrode reactions in solid electrolytes (in Russian). Academy of Sciences of USSR, Ural Dept., Sverdlovsk, pp 80–90
217. Perfilyev MV (1978) Tr Inst Elektrokhim Ural Akad Nauk SSSR 26: 81–87
218. Glumov MV, Neuimin AD, Palguev SF (1968) Elektrokhimiya 4: 1234
219. Glumov MV, Chebotin VN, Palguev SF, Neuimin AD (1970) Elektrokhimiya 6: 391
220. Karpachev SV, Zupnik AE, Perfilyev MV (1970) Elektrokhimiya 6: 577
221. Perfilyev MV (1974) Elektrokhimiya 10: 251
222. Somov SI, Perfilyev MV (1978) In: Physical chemistry of salt melting and solid electrolytes (in Russian). Academy of Sciences of USSR, Ural Dept., Sverdlovsk, pp 95–101
223. Somov SI, Perfilyev MV (1980) Elektrokhimiya 16: 1246
224. Mar'ina OA (1993) PhD Thesis, Russian Academy of Sciences, Sibirian Dept., Novosibirsk
225. Beylaev VD, Sobyanin VA, Mar'ina OA (1990) Izvest Sib Otd Akad Nauk SSSR Ser Khim No 1: 27
226. Mar'ina OA, Sobyanin VA, Belyaev VD (1990) Elektrokhimiya 28: 1413
227. Mar'ina OA, Sobyanin VA, Belyaev VD (1992) Mater Sci Eng B 13: 153
228. Mar'ina OA, Sobyanin VA, Belyaev VD, Parmon VN (1992) Catal Today 13: 61
229. Mar'ina OA, Sobyanin VA (1992) Catal Lett 13: 61
230. Sobyanin VA, Sobolev VI, Belyaev VD, Mar'ina OA, Demin AK, Lipilin AS (1993) Catal Lett 18: 153